Towards Cooperative VRUs: Optimal Positioning Sampling for Pedestrian Awareness Messages

Jorge Martín-Pérez, Oscar Amador, Markus Rydeberg, Linnéa Olsson, Alexey Vinel

Abstract—Road safety is the main motivation for Cooperative Intelligent Transport Systems (C-ITS) in general, and vehicular communications (V2X) technology in particular. The V2X-based Vulnerable Road User (VRU) protection is an approach that relies on the persistent broadcasting of "beacon" awareness messages by a VRU mobile device. To this end the European Telecommunications Standards Institute (ETSI) has specified the Vulnerable Road User Awareness Message (VAM) as well as the overall ITS-G5 protocol stack enabling a variety of the V2X applications. This article studies how often pedestrians (a type of VRU) should check their position to issue a VAM. To that end, we characterize the rate at which pedestrians generate VAMs leveraging a recognized mobility model, and formulate an optimization problem to minimize the time elapsed between VAMs. We propose an algorithm to solve the problem in 802.11p and assess its accuracy through numerical and simulation campaigns. Results evidence the accuracy of our VAM rate characterization, and evidence that we decrease ETSI positioning sampling rate by more than 30%. On top, our solution decreases the time between VAMs, and increases the packet delivery ratio. In other words, our approach increases the pedestrians safety while reducing the battery consumption of mobile devices.

Index Terms—Cooperative Intelligent Transport Systems (C-ITS), Cooperative Vehicles, Automated Driving, Vehicular Communications (V2X), Pedestrian-to-Anything (P2X), Road Safety, Vulnerable Road Users (VRU).

✦

1 INTRODUCTION

O VER 270,000 pedestrians die every year in traffic accidents worldwide [1]. In Europe alone, 19,897 people died in road accidents in 2021 [2]. Pedestrians and cyclists —part of the Vulnerable Road User (VRU) category— make up 27% of those fatalities. These numbers have prompted initiatives such as Vision Zero [3], adopted by the European Commission (EC), which aims at reducing road fatalities and serious injuries to zero by 2050. Furthermore, the United Nations aim to halve the number of deaths/injuries from road traffic accidents by 2030, as specified in [4, Target 3.6] of the Sustainable Development Goals.

- *Jorge Martín-Pérez is with Departamento de Ingeniería de Sistemas Telemáticos, ETSI Telecomunicación, Universidad Politécnica de Madrid, 28040, Spain. Email: jorge.martin.perez@upm.es.*
- *Oscar Amador, Markus Rydeberg, and Linnéa Olsson are with the School of Information Technology, Halmstad University, 30118 Halmstad, Sweden (e-mail:oscar.molina@hh.se, {marryd18,linols18}@student.hh.se*
- *Alexey Vinel is with the Karlsruhe Institute of Technology, 76131 Karlsruhe, Germany*

Technology is one of the fronts that pave the road to Vision Zero. The development of Connected, Cooperative, and Automated Mobility (CCAM) is one of the cornerstones of the technological effort, and VRU protection is one of the main objectives of the industry and research communities working in CCAM. Vehicular communications (V2X) being a part of Cooperative Intelligent Transport Systems (C-ITS) for a plethora of the VRUs types (pedestrians, cyclists, etc.) are central in CCAM framework.

We can divide VRU protection into two main categories: *passive* (when vehicles or the infrastructure detect VRUs) and *active* (when the VRU informs other road users of its presence). In the context of one specific type of the VRU, namely pedestrians, the latter approach is known as Pedestrian-to-Anything (P2X) communication. For an broader overview of the P2X systems, the reader is referred to the most recent survey [5].

For P2X, standardization bodies such as Society of Automotive Engineers (SAE) International and the European Telecommunications Standards Institute (ETSI) have specified two services powered by beacon messages: the SAE Personal Safety Message (PSM) [6], and the ETSI Vulnerable Road User Awareness Message (VAM) [7]. There is already some work in the literature assessing the efficiency of PSM [8] and VAM [9]–[12]. The congestion in a broadcast communication channel, i.e., when many nodes (e.g., VRUs, vehicles) contend for the medium has a non-negligible effect on the beacon messages delivery. It is already exhibited in works related to vehicles broadcasting Cooperative Awareness Messages (CAMs) [13] [14]. Congestion effects can be expected to become even more prominent in case of pedestrians sending VAMs due to their potentially higher density in comparison to vehicles.

ETSI VAMs may congest the channel upon high VRU

(a) VAMs are sent when pedestrians move Δ meters at speed σ.

(b) VAMs are sent when pedestrians change their speed σ (in m/sec).

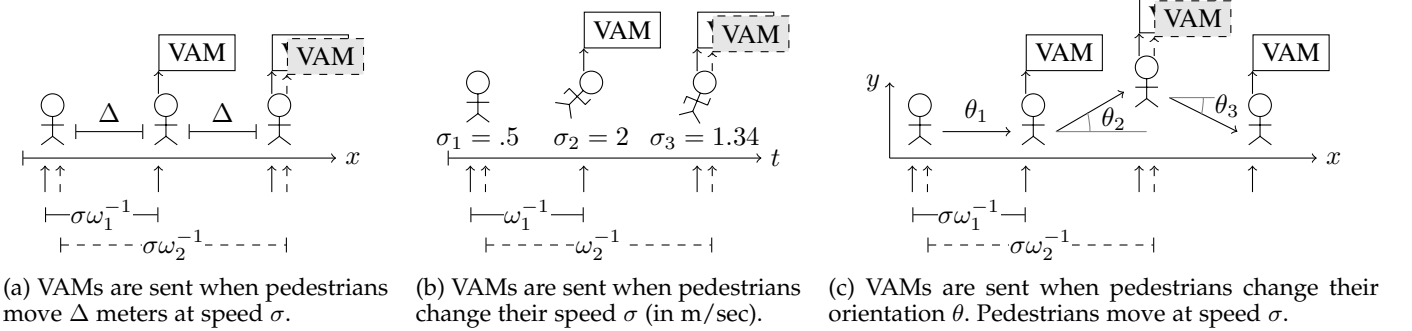(c) VAMs are sent when pedestrians change their orientation θ. Pedestrians move at speed σ.

Fig. 1: VAMs generated by a pedestrian moving to the right. At the bottom we illustrate the positioning checks (arrows) at high frequency ω_1 Hz (solid) and low frequency ω_2 Hz (dashed). On top we illustrate the VAMs generated due to high frequency (solid) and low frequency checks (dashed).

density or large VAM generation rates. According to ETSI [7], pedestrians and other VRUs should generate a VAM if there is a change of position, heading, or speed. In particular, VRUs must sample their position at a rate above 10 Hz to check if a VAM must be generated [7].

Despite the existing literature assessing the performance of VRU VAMs [9]–[12], to the best of our knowledge there exists only one work evaluating ETSI VA parameters regarding the generation of VAMs. In particular, [15] evaluates how ETSI parameters impact the performance of VAMs within VRU clusters. However, still there is no study on how the positioning sampling impacts the rate at which VAMs are successfully received.

In this work we argue whether the positioning sampling rate proposed by ETSI (10 Hz) [7] is optimal to ensure pedestrian VAMs are delivered upon channel congestion. Namely, we investigate whether it is even possible to decrease the positioning sampling rate to generate less VAMs and prevent congestion, yet minimizing the time elapsed between received pedestrian VAMs. Our work sets forth the following contributions:

- In §3–5, we characterize how the positioning sampling rate impacts the rate at which pedestrians generate ETSI VAMs due to: position changes (§3), speed changes (§4), and heading/orientation changes (§5).
- In §6, we formulate an optimization problem to find the positioning sampling rate minimizing the time elapsed between pedestrian VAM receptions. Our formulation accounts for the channel congestion. Moreover, we leverage our VAM characterization and propose an algorithm to find the optimal positioning sampling rate for 802.11p (§6.1).
- In §7, we (*i*) show that our VAM characterization is conservative with an error below 0.157 VAMs/sec (§7.1); and (*ii*) show through 802.11p numerical/simulation results how our algorithm minimizes the time between pedestrian VAMs decreasing a 30% ETSI positioning sampling rate (§7.2 and 7.3).

The motivation behind using 802.11p is three-folded: its integration in cars (e.g., Volkswagen ID.4, and a fleet of Renault cars [16]) and implementation of commercial On-board Units [17]; the existence of a closed-form analytical model of the channel access [18]; and the stability of the Artery/Veins/SUMO [19]–[21] stack to emulate ETSI VRUs

TABLE 1: Notation Table

Symbol	Definition
ω	Positioning sampling frequency
$x(t)$	Pedestrian position at time t
$\sigma(t)$	Pedestrian speed at time t
$\theta(t)$	Pedestrian orientation at time t
Δ	Position difference threshold
δ_σ	Speed difference threshold
δ_θ	Orientation difference threshold
$\lambda_\Delta(\omega)$	Rate of position change VAMs with sampling ω
$\lambda_\sigma(\omega)$	Rate of speed change VAMs with sampling ω
$\lambda_\theta(\omega)$	Rate of orientation change VAMs with sampling ω
$\lambda(\omega)$	Total VAM rate with sampling ω

and VAMs on top of 802.11p. Nevertheless, it is possible to adapt our solution to technologies as 802.11bd or C-V2X – see the end of §6.1 for further details.

2 OVERVIEW OF ETSI VAM GENERATION RULES

VAMs are generated depending on VRU kinematic triggers. The interval between two VAMs (*T_GenVam*) is in between 0.1 sec (*T_GenVamMin*) and 5 sec (*T_GenVamMax*) – see [7, Table 16]. VRUs must check at least every *T_GenVamMin* seconds whether a VAMs should be generated [7, 6.2]. That is, VRUs check their position at a rate $\omega \geq 1/T\_GenVamMin$.

A VAM is generated by either of two conditions:

1) the VRU exceeds a set of kinematic thresholds with respect to the last VAM:
   (a) its position (x) changed by more than *minReferencePointPositionChangeThreshold* (Δ) meters;
   (b) its speed (σ) changed by more than *minGroundSpeedChangeThreshold* (δ_σ) m/sec; or
   (c) its orientation (θ) changed by more than *minGroundVelocityOrientationChangeThreshold* (δ_θ) degrees; or
2) the time since the last VAM exceeds *T_GenVamMax* and rules for redundancy mitigation are met (e.g., if the VRU is not stationary, up to 10 VAMs can be skipped).

Fig. 1 illustrates the VAMs that pedestrians generate due to the aforementioned kinematic thresholds — i.e. (a), (b), and (c). The values set by ETSI [7, Table 17] are $\Delta = 4$ meters, $\delta_\sigma = 0.5$ m/sec and $\theta = 4$ degrees.

A VRU will trigger more VAMs if it checks more frequently its position, thus the triggering conditions.
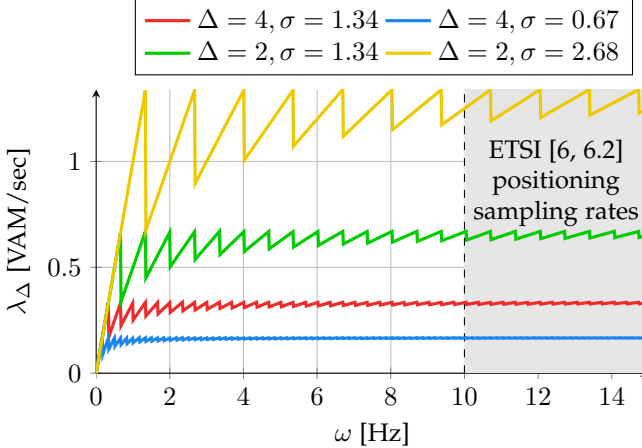
Fig. 2: VAM generation rate due to position changes λ_Δ increases in a saw teeth fashion with the positioning sampling rate ω. The smaller the distance Δ and the larger the speed σ, the larger λ_Δ. We assume a constant speed σ.

For example, the VRU generates more VAMs with $T\_GenVamMin = 100\,\text{ms}$ ($\omega = 10\,\text{Hz}$) than with $T\_GenVamMin = 1\,\text{sec}$ ($\omega = 1\,\text{Hz}$). This is because it is more likely to envision changes of position, speed or orientation if the position is sampled more often. In other words, the VAM rate of a pedestrian $\lambda(\omega)$ is monotonically increasing on the checking rate — i.e. $\lambda(\omega_1) \leq \lambda(\omega_2)$ with $\omega_1 \leq \omega_2$.

Having high VAM rates helps to have more accurate and real time information about where pedestrians are, how fast they move and where they are heading to. However, high VAM rates may result in collisions in the wireless medium when using technologies as 802.11p. Therefore, in this article we look for the best positioning sampling rate ω to have accurate information about the VRU, yet preventing the collision of the VAMs.

Before looking for the best positioning sampling rate ω, in the following sections we characterize the rate of VAMs due to position changes in §3, speed changes in §4 and orientation changes in §5.

3 VAMs UPON POSITION CHANGES

As stated in §2, VRUs check at a rate ω whether they have moved Δ meters or not. If the VRU travels at speed σ meters/sec, each checking period it travels $\sigma\omega^{-1}$ meters – as illustrated in Fig.1a. Moreover, it takes $\lceil \omega\Delta/\sigma \rceil$ positioning samples to realize that a pedestrian exceeded Δ meters. As a result, the rate at which a pedestrian generates VAMs due to position changes is

$$\lambda_\Delta(\omega) = \omega \left\lceil \frac{\omega\Delta}{\sigma} \right\rceil^{-1} \qquad (1)$$

The VAM generation rate λ_Δ upon position changes exhibits a saw-teeth behaviour that depends on the checking distance Δ, speed σ and checking frequency ω. Fig. 2 illustrates the saw-teeth tendency and highlights how position VAMs are generated more frequently if the average speed increases. That is, it is more likely to realize a change of Δ meters in the position if the pedestrian moves faster.

Note that in (1) we assume constant speeds for pedestrians. The assumption is supported by the rather negligible speed variations that we foresee in §4 analysis. Despite the assumption, Fig. 2 evidences that the rate of positioning VAMs λ_Δ stabilizes at rather small values of ω – e.g. around $\omega = 2$ for average pedestrian speeds [22] of $\sigma = 1.34\,\text{m/sec}$ and the standard [7] $\Delta = 4$ meters. Hence, upon rather constant speeds pedestrians can decrease the rate at which they check the positioning without harnessing the generation of VAMs upon changes of positions. In other words, as Fig. 2 illustrates, it is not necessary to set $\omega \geq 10\,\text{Hz}$ – as specified by ETSI in [7, 6.2].

4 VAMs UPON SPEED CHANGES

In the previous section we consider that VRUs travel at a constant speed σ m/sec to derive the rate of VAMs generated because the VRU position changes by more than Δ meters. In real-world the VRUs vary their speed and we should consider a time dependent variable $\sigma(t)$.

A speed change will trigger a VAM if $|\sigma(i\omega^{-1}) - \sigma(i_0\omega^{-1})| \geq \delta_\sigma$ holds for $i > i_0 \geq 0$ – with δ_σ the *minGroundSpeedChangeThreshold* defined in [7]. That is, a VAM is generated if at the ith sample the speed changed by more than $\delta_\sigma = 0.5\,\text{m/sec}$ [7] with respect to the speed at the i_0^{th} sample.

We resort to the Gradient Navigation Model (GNM) [23] to understand how pedestrians move and change their speed $\sigma(t)$ over time. According to the GNM, every pedestrian movement is affected by the neighboring pedestrians, e.g. a pedestrian will not move to the right if there is another person at its near right; otherwise it would clash with that person. We refer to $N(t) \in \mathbb{R}^2$ as the desired direction of a pedestrian given its neighbors movement and the obstacles around it, which is defined in [23] as

$$N(t) = g\left(g(N_T) + g(N_P)\right) \qquad (2)$$

with $g : \mathbb{R}^2 \mapsto \mathbb{R}^2$, $\|g(x)\| \leq 1, \forall x$, N_T the target vector (where the pedestrian goes), and N_P the perturbance of neighboring pedestrians – see [23, (2),(A4)] for the precise definitions of N_P and $g(x)$, respectively

According to [23], the speed vector at a given time $\dot{x}(t)$ is given by the product of the target vector – with norm (2), $\|N(t)\| \leq 1$ – and the relaxed speed $w(t)$ that the pedestrian has. Hence, the Ordinary Differential Equations (ODE) system is

$$\dot{x}(t) = w(t)N(t) \qquad (3)$$

$$\dot{w}(t) = \frac{1}{\tau}\left(v\|N(t)\| - w(t)\right) \qquad (4)$$

with v the desired speed, and τ the speed of reaction of a pedestrian, i.e. how long it takes to adapt her speed.

Note that the ODE system in (3)-(4) fully determines what is $\sigma(i\omega^{-1}) = \|\dot{x}(i\omega^{-1})\|$ and it is enough to resort to approaches as the Euler method or Dormand-Prince-45 [24] to find $\sigma(i\omega^{-1})$.

Given a reference sample when the last VAM was generated i_0, it is possible to know when the speed will change by more than δ_σ m/sec. In particular, we obtain the time to the next VAM due to a speed change as $\omega^{-1}\inf_{i>i_0}\left\{\left|\sigma(i\omega^{-1}) - \sigma(i_0\omega^{-1})\right| \geq \delta_\sigma\right\}$. That is, we evolve the ODE system until the first sample $i > i_0$ at which the speed change exceeds δ_σ. Consequently, we estimate the
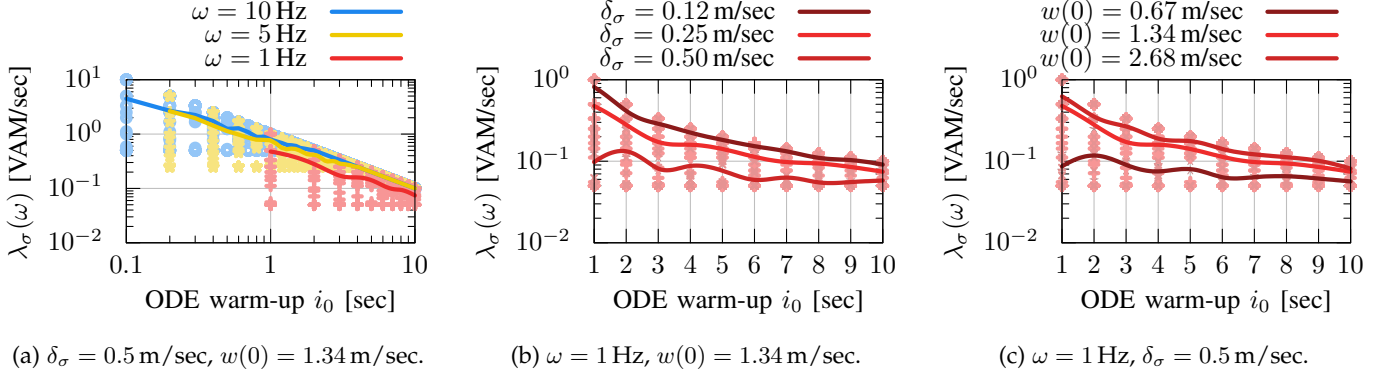
Fig. 3: Speed VAM generation rate $\lambda_\sigma(\omega)$ vs. the pedestrian GNM [23] warm-up time i_0. Pedestrians have reaction time $\tau = 0.5\,\mathrm{sec}$ and desired speed $v = 1.34\,\mathrm{m/sec}$. We try out different: (a) checking rates ω; (b) *minGroundSpeedChangeThreshold* δ_σ; and (c) initial speeds $w(0)$. We illustrate the VAM rate for each random trajectory of the ODE system (points), and the average VAM rate (lines).

rate of VAMs due to speed changes as the inverse of the time until the next VAM occurs given the reference sample i_0

Lemma 1 (VAM rate due to speed changes). *A pedestrian with initial speed $w(0)$, reaction time τ, sampling rate ω and desired speed v generates VAMs due to speed changes at rate*

$$\lambda_\sigma(\omega) = \omega\Bigg(\inf_{i>i_0}\Big\{\big|N_i a^{\frac{i}{h\omega}} w(0)$$

$$+ v\frac{1-a}{a}N_i \sum_{m=0}^{\frac{i}{h\omega}} a^{\frac{i}{h\omega}-m}N_{mh} - w(i_0\omega)N_{i_0}\big| \geq \delta_\sigma\Big\}\Bigg)^{-1} \quad (5)$$

with $a = 1 - \frac{h}{\tau}$, $N_i = \|N(ih)\|$ and $h < \tau$ the Euler method step size.

Proof. Using the Euler method in the ODE system (3)-(4) we obtain $w(t)$ by induction.

Considering the step size $h > 0$ we have a one step progression

$$w(h) = w_0\left(1 - \frac{h}{\tau}\right) + \frac{hv}{\tau}\|N(0)\| = w(0)a + v(1-a)N_0 \quad (6)$$

If we take another step it is easy to show that

$$w(2h) = a^2 w(0) + v(1-a)\left(aN_0 + N_h\right) \quad (7)$$

so we obtain $w(kh)$ by induction on k

$$w(kh) = a^k w(0) + v\frac{1-a}{a}\sum_{m=0}^{k} a^{k-m}N_{mh} \quad (8)$$

By doing a change of variable $t = kh$ and then taking $t = i\omega^{-1}$ in (8) we get

$$w(i\omega^{-1}) = a^{\frac{i}{h\omega}}w(0) + v\frac{1-a}{a}\sum_{m=0}^{\frac{i}{h\omega}} a^{\frac{i}{h\omega}-m}N_{mh} \quad (9)$$

and (5) holds since $\sigma(i\omega^{-1}) = w(i\omega^{-1})N_i$ □

Although it may seem like Lemma 1 provides an intractable expression for $\lambda_\sigma(\omega)$, it allows us to understand the dynamics of a pedestrian. In particular, we observe how

it becomes more difficult to exceed the *minGroundSpeedChangeThreshold* parameter δ_σ as we increase i_0 (the ODE warm-up time). This is mainly because the term a is below one and it is powered to $i > i_0$. Hence, the speed differences reduce as time passes.

Moreover, given that $\|N(t)\| \leq 1$ it is possible to randomize the target vector and estimate $\lambda_\sigma(\omega)$. Specifically, we i) take random realizations of $N_{i_0}, N_{i_0+1}, \ldots$; and ii) compute $\lambda_\sigma(\omega)$ for each random realization. Each random realization gives a possible trajectory of he pedestrian corresponding to a set of initial conditions. Thus, we resort to the average of such random realizations to estimate $\lambda_\sigma(\omega)$.

In Fig. 3 we illustrate how the speed VAMs rate estimation changes with respect to the ODE warmup i_0, sampling rate ω, δ_σ, and initial speed $w(0)$. Results show the aforementioned phenomena of having smaller rate as the ODE warmup increases. On top, results also evidence that the higher the sampling rate ω, the higher the VAM rate due to speed changes $\lambda_\sigma(\omega)$ because more checks can detect more speed changes.

Later, in §7.1, we show that the randomized approach to estimate $\lambda_\sigma(\omega)$ results into upper bounds for the rate of VAMs generated in a validated mobility simulator implementing the GNM [23]. Such upper bounds hold for rates above $\omega = 10^{-1}\,\mathrm{Hz}$, thus covering the range of sampling rates considered by ETSI [7] $\omega \geq 10\,\mathrm{Hz}$.

5 VAMs UPON ORIENTATION CHANGES

In this section, we want to know the rate at which VAMs are generated due to orientation changes. That is, the VAMs generated when the user orientation $\theta(t)$ changed more than $\delta_\theta = 4$ [7] with respect to the orientation reported in the last VAM at time $\theta(i_0\omega^{-1})$.

Without loss of generality we take as reference the vector $(1, 0)$, hence define the orientation at time $t = i\omega^{-1}$ as

$$\theta(i\omega^{-1}) = \arccos\left(\frac{(x(i\omega^{-1}) - x((i-1)\omega^{-1})) \cdot (1, 0)}{|x(i\omega^{-1}) - x((i-1)\omega^{-1})|}\right) \quad (10)$$

To obtain what will be the orientation (10) at time $i\omega^{-1}$ we resort to the GNM [23] ODE system in (3)-(4).
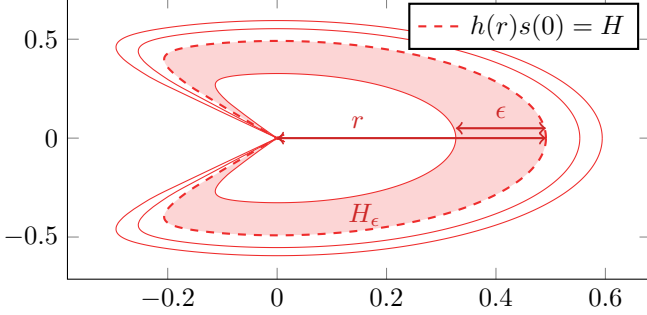
Fig. 4: Isolines of influence $h(r)s(\theta)$ for a pedestrian at the origin moving to the right. H_ϵ refers to the band of influence of width ϵ w.r.t. isoline of magnitude H.

Fig. 5: A pedestrian at the origin experiences repulsive forces ∇P_k from the wall and two pedestrians x_i, x_j. As a result, the GNM [23] shifts her orientation $g(N_T)$ by θ degrees.

With the orientation $\theta(i\omega^{-1})$, $i > 0$ we then obtain the rate of VAMs due to orientation changes λ_θ. In particular, in §5.1 we explain how pedestrians and obstacles influence the pedestrian position. Then, in §5.2 we obtain the average change of orientation that a pedestrian experiments when neighbors coordinates follow a Poisson Point Process (PPP). Lastly, in §5.3 we use the average change of orientation to derive the rate of VAMs due to speed changes λ_θ.

5.1 Influence of Neighboring Pedestrians

As shown in (10), the change of orientation is computed taking the difference between the current position $x(i\omega^{-1})$ and the prior position $x((i-1)\omega^{-1})$. Based on the GNM (3), the direction of the position vector $x(t)$ is fully determined by the pedestrian desired direction $N(t)$.

The pedestrian desired direction $N(t)$ is impacted (2) by repulsive forces induced by neighboring pedestrians ∇P_i and obstacles ∇P_b. The negative sum of such repulsions results in the repulsive forve $N_P(t) = g(-\sum_k \nabla P_k)$ that alters the pedestrian desired direction – see Fig. 5.

According to [23], the repulsion induced by a neighboring pedestrian i is

$$\nabla P_i = h\left(\|x_i\|; p_i, R_i\right) s(\theta_i) \frac{x_i}{\|x_i\|} \quad (11)$$

with $h(\cdot)$ a monotonically decreasing function w.r.t. the distance taking its maximum at p_i and zero for values above R_i – see [23, (3)]– and $s(\theta_i)$ the repulsion of neighbors depending on the angle angle θ_i w.r.t. pedestrian i – see [23, (4)].

Fig. 4 shows the isolines of influence (11) experienced by a pedestrian at the origin. The isolines $h(\cdot)s(\cdot) = H$ evidence a cardioid shape that capture how a pedestrian does not experience repulsion $\nabla P_i = 0$ if the pedestrian i is behind her.

Note that in (11) we consider that the pedestrian of interest is located at the origin $x_0 = (0,0)$ and the original expression for $h(\|x_i - x_0\|; p_i, R_i)$ in [23, (5)] is simplified to (11). Additionally, we also use (11) to define the repulsion ∇P_b induced by an obstacle b as the wall in Fig. 5, with the peculiarity of replacing p_i, R_i by p_b, R_b – i.e. the maximum value and support of the function $h(\cdot)$.

Overall, we compute the desired direction at a given time $N(t)$ in (10) using the pedestrian direction N_T, neighbors/obstacles repulsion $N_P = -\sum_b \nabla P_b - \sum_i \nabla P_i$ and
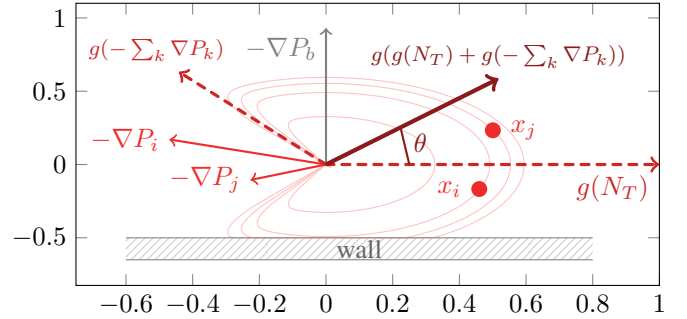
the normalizing function $g : \mathbb{R}^2 \to \mathbb{R}^2$ with $\|g(x)\| \in [0,1]$ – see its definition in [23, Appendix A]. Consequently, we can obtain the change of orientation by replacing $x(t)$ with $N(t)$ in (10), since the pedestrian position $x(t)$ direction is fully determined by $N(t)$ – see (3).

In Appendix A we try to bound the orientation $\theta(i\omega^{-1})$ hoping that the orientation of a user stabilizes as time evolves, hence resulting into $\lambda_\theta \simeq 0$. For we could not find any bound, in §5.2 we use the pedestrians repulsion ∇P_i to compute the average change of orientation $\mathbb{E}[\theta((i+k)\omega^{-1}) - \theta(i\omega^{-1})]$ and get the rate of orientation change VAMs λ_θ.

5.2 Average Change of Orientation

In this section we compute the average change of orientation $\mathbb{E}[\theta((i+k)\omega^{-1}) - \theta(i\omega^{-1})]$ as follows

i) we consider that pedestrians [25] coordinates follow an homogeneous PPP with average rate μ ped/m²;
ii) we compute the average force that pedestrians induce in a band of influence $\nabla P(H_\epsilon, k)$ when the pedestrian is d meters away from a wall – see Fig. 4 and Fig. 5; and
iii) we average the influence of each band H_ϵ to obtain the average change of orientation.

Following the lead of [26], we consider that pedestrians coordinates are goberned by an homogeneous PPP $\Phi = \{x_j\}_{j \in \mathbb{N}}$ of rate μ. Hence, we know [25] the probability of having k pedestrians within the band H_ϵ is precisely $\mathbb{P}(N(H_\epsilon) = k) = (\mu|H_\epsilon|)^k/k! \cdot e^{-\mu|H_\epsilon|}$, with $|H_\epsilon|$ being the area for the band of width ϵ starting at the isoline $h(r)s(\theta) = H$ (see Fig. 4).

However, sometimes the pedestrian is near an obstacle as a wall and the area of the band H_ϵ is clipped by the the wall – see Fig. 5. Hence the area of the band of influence given that a wall is d meters away is

$$|H_\epsilon(d)| = \int_0^{2\pi} \int_{r(\theta,H)}^{r(\theta,H+\epsilon)} \rho \cdot \mathbb{1}_{[-d,\infty)}(\rho\sin(\theta)) \, d\rho \, d\theta \quad (12)$$

with $r(\theta, H) \in \mathbb{R}^+$ a function that maps the distance at which is the isoline H with polar coordinates θ, $\mathbb{1}_A(x)$ the indicator function taking value one if $x \in A$ and zero otherwise. We refer the reader to (40) in Appendix B for a detailed definition of $r(\theta, H)$.

Note that (12) only considers the case of a wall bellow the pedestrian, as illustrated in Fig. 5. In case there are two

walls surrounding a sidewalk (or the start of a road and a wall), we apply (12) in one half of the sidewalk, and the same expression in the other half.

Given the area of the band $H_\epsilon(d)$, we can obtain a closed-form expression for the average influence of neighbors within such band.

Lemma 2 (Average band influence). *Given a pedestrian d meters away from a wall/obstacle and a bounding box $B \subset \mathbb{R}^2$, the average influence of the band $H_\epsilon \subset B$ is*

$$\mathbb{E}[\nabla P(H_\epsilon, d)] = \sum_{n=0}^{\infty} \sum_{k=0}^{n} \left(\mathbb{E}[\nabla P(H_\epsilon, k, d)] \right.$$
$$\left. \cdot \frac{\mu^{2n} |H_\epsilon|^k |\overline{H}_\epsilon|^{n-k} |B|^n}{n! k! (n-k)!} e^{-2\mu|B|} \right) \quad (13)$$

with $\overline{H}_\epsilon = B \setminus H_\epsilon$, and $\nabla P(H_\epsilon, k, d)$ the average influence of band H_ϵ with an obstacle/wall d meters away and with k pedestrians inside

$$\mathbb{E}[\nabla P(H_\epsilon, k, d)]$$
$$= \int_0^{2\pi} \frac{k \, h(r(\theta, H\frac{\epsilon}{2})) s(\theta) g_\epsilon(\theta, H, d)}{2\pi} (\cos\theta, \sin\theta) \, d\theta \quad (14)$$

with $g_\epsilon(\theta, H, d) = \mathbb{1}_{[-d,\infty)}(r(\theta, \frac{H+\epsilon}{2}) \sin\theta)$

Proof. First we compute $\mathbb{E}[\nabla P(H_\epsilon, k, d)]$. Without loss of generality, we consider that the a pedestrian within the band of influence H_ϵ is at the isoline $H_\epsilon + \frac{\epsilon}{2}$ – i.e. at the middle – for $\epsilon > 0$ small enough. Such pedestrian j would have polar coordinates $x_j = (r(\theta_j, H_\epsilon + \frac{\epsilon}{2}), \theta_j) = (r_j, \theta_j)$ and its ocurrence would have probability $\mathbb{P}(\Phi = x_j | N(H_\epsilon) = k) = \frac{k}{2\pi}$

According to (11), the pedestrian j would induce a repulsion $\nabla P(\theta_j) = h(r_j, \theta_j) s(\theta_j) x_j / r_j$ as long as x_j is not at the other side of the wall at distance d, i.e. as long as $g_\epsilon(\theta_j, H, d) = 1$. Consequently, the average influence of band H_ϵ is

$$\mathbb{E}[\nabla P(H_\epsilon, k, d)] = \mathbb{E}_\Phi[\nabla P(H_\epsilon, k, d) | N(H_\epsilon) = k]$$
$$= \int_0^{2\pi} \nabla P(\theta_j) \, \mathbb{P}(\Phi = x_j | N(H_\epsilon) = k) \, d\theta_j \quad (15)$$

wich results into (14) in cartesian coordinates.

Now we compute what is the average band influence resorting to the PPP density function:

$$\mathbb{E}[\nabla P(H_\epsilon, d)]$$
$$= \sum_{n}^{\infty} \mathbb{E}[\nabla P(H_\epsilon, d) | N(B) = n] \, \mathbb{P}(N(B) = n)$$
$$= \sum_{n}^{\infty} \sum_{k=0}^{n} \mathbb{E}[\nabla P(H_\epsilon, d) | N(H_\epsilon) = k, N(B) = n]$$
$$\cdot \mathbb{P}(N(H_\epsilon) = k | N(B) = n) \, \mathbb{P}(N(B) = n)$$
$$= \sum_{n}^{\infty} \sum_{k=0}^{n} \mathbb{E}[\nabla P(H_\epsilon, k, d)]$$
$$\cdot \mathbb{P}(N(H_\epsilon) = k, N(\overline{H}_\epsilon) = n-k) \, \mathbb{P}(N(B) = n)$$
$$\quad (16)$$

which yields (13) using the PPP density function. $\qquad \square$

Thanks to Lemma 2 we can approximate, on average, the change of orientation. Specifically, we compute the change of orientation with a wall/obstacle d meters away.

Lemma 3 (Average Change of Orientation). *A pedestrian d meters away from the wall experiences an average change of orientation*

$$\mathbb{E}\left[\theta((i+k)\omega^{-1}) - \theta(i\omega^{-1}) | \, d\right]$$
$$= \arccos\left(\frac{g_1(-\nabla P_b - \mathbb{E}[\nabla P(H_\epsilon, d)])}{\|g(-\nabla P_b - \mathbb{E}[\nabla P(H_\epsilon, d)])\|}\right) - \theta(i\omega^{-1}) \quad (17)$$

with $k > 0, i \geq 0$; and $g_1(\cdot)$ the first coordinate of $g(\cdot)$; $\nabla P_b = (0, h(d; p_b, R_b))/d$ the wall repulsion [23, (6)] with p_b, R_b the maximum and support of $h(\cdot)$.

Proof. For $\theta(i\omega^{-1})$ refers to the current orientation of the pedestrian, all we have to compute is the average orientation at time $(i+k)\omega^{-1}$

$$\mathbb{E}[\theta((i+k)\omega^{-1}) | \, d]$$
$$= \mathbb{E}\left[\arccos\left(\frac{x_1((i+k)\omega^{-1}) - x_1((i+k-1)\omega^{-1})}{\|x((i+k)\omega^{-1}) - x((i+k-1)\omega^{-1})\|}\right)\right]$$
$$\quad (18)$$

Now we obtain the average change of position as follows

$$\mathbb{E}[x((i+k)\omega^{-1}) - x((i+k-1)\omega^{-1}) | \, d]$$
$$= x(i\omega^{-1}) + k\omega^{-1}\mathbb{E}[w((i+k)\omega^{-1})]\mathbb{E}[N_P | \, d]$$
$$- x(i\omega^{-1}) - (k-1)\omega^{-1}\mathbb{E}[w((i+k-1)\omega^{-1})]\mathbb{E}[N_P | \, d]$$
$$= \frac{\overline{w}}{\omega} g(-\nabla P_b - \mathbb{E}[\nabla P(H_\epsilon, d)]) \quad (19)$$

with the first equality holding by taking a $k, k-1$ sized step in the Euler method and the ODE system in (3); $\overline{w}$ the average speed of a pedestrian – approximately $1.34 \, \text{m/sec}$ [23]; and $g(\cdot)$ the vector normalization in [23, Appendix 1]. Note that plugging (19) into (18) results into (17). $\qquad \square$

Thanks to Lemma 3, in the next section §5.3 we obtain the average rate of VAMs generated due to change of orientations.

5.3 Average Rate of VAMs Upon Change of Orientation

With the average orientation we now compute what is the average rate of VAMs that any pedestrian would generate due to changes of orientation – i.e. when $|\mathbb{E}[\theta((i+k)\omega^{-1}) | \, d] - \theta(i\omega^{-1})| > \delta_\theta$ occurs. In particular, we approximate λ_θ assuming that speed change VAMs are negligible $\lambda_\sigma(\omega) \to 0$. Such assumption holds — as evidenced in §7.1 – due to the tendency of having less speed changes as the ODE warmup increases. Notice how $\lambda_\sigma(\omega) \to 0$ as $i_0 \to \infty$ in Lemma 1.

Before obtaining λ_θ it is worth mentioning that the change of orientation is computed against the orientation reported in the last VAM. Consequently, if a change of position VAM occurs before a change of orientation — let us say at time $t = 3\omega^{-1}$ — the next check for the orientation check is computed as $|\mathbb{E}[\theta(4\omega^{-1}) | \, d] - \theta(3\omega^{-1})|$ which we can approximate as $|\mathbb{E}[\theta((i+1)\omega^{-1}) | \, d] - \theta(i\omega^{-1})|$. Therefore, a VAM due to a change of orientation must happen before a VAM due to a change of position, which happens each each $\omega \lceil \omega \Delta/\sigma \rceil$ sec.

Consequently, we approximate the probability of sending an orientation change VAM at the kth sampling period as

$$
\begin{aligned}
p_\theta(k) &= \int_{d_m}^{d_M} \frac{\mathbb{1}_{>\delta_\theta}\left(|\mathbb{E}[\theta((i+k)\omega^{-1})|x] - \theta(i\omega^{-1})|\right)}{d_M - d_m} dx \\
&= \int_{d_m}^{d_M} \frac{\mathbb{1}_{>\delta_\theta}\left(|\mathbb{E}[\theta(k)|\,x] - \theta(0)|\right)}{d_M - d_m} dx, \quad k \le \left\lceil \frac{\Delta\omega}{\sigma} \right\rceil
\end{aligned} \tag{20}
$$

as long as k is below the number of samples it takes to trigger a VAM due to a change of position – i.e. as long as $k \le \lceil \Delta\omega/\sigma \rceil$.

Knowing that VAMs due to position changes restart the check of the orientation change, we obtain the average rate of VAMs due to orientation changes in the next Lemma.

Lemma 4 (Average rate of orientation VAMs). *A pedestrian with average speed σ and positioning sampling rate ω sends orientation change VAMs at an average rate λ_θ whose inverse satisfies*

$$
\mathbb{E}[\lambda_\theta^{-1}] = \frac{\omega^{-1}}{1 - p_{err}} \left(p_1 + \frac{I_\Delta p_0 p_{err}}{1 - p_{err}} \right) \tag{21}
$$

with $I_\Delta = \lceil \Delta\omega/\sigma \rceil$ and p_0, p_1, p_{err} as defined in (25)-(27).

Proof. We first compute what is the probability of a orientation VAM occurring at the kth sampling period

$$
\mathbb{P}(\lambda_\theta^{-1} = k\omega^{-1}) = p_\theta(k) \prod_{m=1}^{k-1} (1 - p_\theta(m)), \quad k < I_\Delta \tag{22}
$$

with $I_\Delta = \lceil \Delta\omega/\sigma \rceil$ the number of sampling periods ω^{-1} required to trigger a position VAM.

Next, we compute the probability of an orientation VAM occuring at the kth sampling period after the jth position VAM

$$
\begin{aligned}
&\mathbb{P}\left(\lambda_\theta^{-1} = (jI_\Delta + k)\,\omega^{-1}\right) \\
&= \left(\prod_{m=1}^{I_\Delta} (1 - p_\theta(m))\right)^j \mathbb{P}(\lambda_\theta^{-1} = k\omega^{-1}), \quad k < I_\Delta
\end{aligned} \tag{23}
$$

Then we compute the average rate as

$$
\mathbb{E}[\lambda_\theta^{-1}] = \sum_{j=0}^{\infty} \sum_{k=1}^{I_\Delta - 1} \frac{jI_\Delta + k}{\omega} \mathbb{P}\left(\lambda_\theta^{-1} = (jI_\Delta + k)\,\omega^{-1}\right) \tag{24}
$$

If we call

$$
p_0 = \sum_{k=1}^{I_\Delta - 1} \mathbb{P}(\lambda_\theta^{-1} = k\omega^{-1}) \tag{25}
$$

$$
p_1 = \sum_{k=1}^{I_\Delta - 1} k\mathbb{P}(\lambda_\theta^{-1} = k\omega^{-1}) \tag{26}
$$

$$
p_{err} = \prod_{m=1}^{I_\Delta} (1 - p_\theta(m)) \tag{27}
$$

expression (24) becomes

$$
\begin{aligned}
\mathbb{E}[\lambda_\theta^{-1}] &= \omega^{-1} \sum_{j=0}^{\infty} \sum_{k=1}^{I_\Delta - 1} (jI_\Delta + k) p_{err}^j \mathbb{P}(\lambda_\theta^{-1} = k\omega^{-1}) \\
&= \omega^{-1} \sum_{j=0}^{\infty} p_{err}^j (jI_\Delta p_0 + p_1) \\
&= \omega^{-1} \left(\frac{I_\Delta p_0 p_{err}}{(1 - p_{err})^2} + \frac{p_1}{1 - p_{err}} \right)
\end{aligned} \tag{28}
$$

$\square$

6 PEDESTRIAN IPG MINIMIZATION

In this section we describe which is the adequate sampling rate ω to minimize the average Inter Packet Gap (IPG) of VAMs. Decreasing the IPG results into increasing the rate at which VAMs are received, hence resulting into fresh information regarding the pedestrians' positions. In particular, we are interested into decreasing the IPG of VAMs belonging to Profile 2 VRUs [7], i.e. the IPG between pedestrian VAMs. From now on we will refer to the pedestrian VAMs' IPG as pIPG.

To obtain the average pIPG we resort to the rate at which pedestrians send traffic. Each pedestrian sends an average rate of $\lambda(\omega) = \lambda_\Delta + \lambda_\sigma(\omega) + \lambda_\theta(\omega)$ VAM/sec that we obtain using (1), Lemma 1, and Lemma 4; respectively. On top, other VRUs (e.g. bikes) and vehicles (e.g. cars) send their corresponding VAM and CAM messages over the wireless channel. We refer to λ_b, λ_c as the average rate of VAMs of other VRUs as bikes, and the average rate of CAMs of vehicles as cars – thus, the subscripts. Similarly, we refer to n_p as the number of pedestrians sending VAMs, n_b as the number of bikes (other VRUs) sending VAMs, and n_c as the number of vehicles sending CAMs.

Consequently, the wireless channel foresees the following average aggregated rate of VAMs and CAMs

$$
\Lambda(\omega) = \lambda_b n_b + \lambda_v n_v + \lambda(\omega) n_p = \Lambda_v + \Lambda_b + n_p \lambda(\omega) \tag{29}
$$

with Λ_v, Λ_b the total rate of other VRUs and vehicles. Note that it is possible to estimate both n_b, n_v and λ_b, λ_v either from an RSU, or with estimations carried over time as the device listens to the wireless channel. Even if a VAM/CAM is lost due to collisions, it is possible to infer the rate checking the identifiers of the successfully received VAMs/CAMs.

To derive the pIPG we resort to the following lemma.

Lemma 5 (VRU average pIPG). *And VRU with checking frequency ω, speed σ, checking distance Δ experiencing a PDR $p(\Lambda(\omega))$ foresees an average pIPG:*

$$
\mathbb{E}[\text{pIPG}] = \frac{1}{n_p \lambda(\omega) p(\Lambda(\omega))} \tag{30}
$$

with n_p the number of active pedestrian VRUs, $\lambda(\omega)$ their average VAM rate, and $p(\Lambda(\omega))$ the PDR in the wireless medium due to the global VAM/CAM rate upon a sampling frequency ω.

Proof. The wireless channel foresees an aggregated rate of $n_p \lambda(\omega)$ VAM/sec from pedestrians. Hence, the average time ellapsing between pedestrian VAMs is $\frac{1}{n_p \lambda(\omega)}$ sec. However, it may happen that a pedestrian VAM is lost with probability

$1 - p(\Lambda(\omega))$, with the latter term referring to the PDR due to the aggregate VAM rate in the channel, considering that pedestrians have a sampling rate ω. Consequently, the probability of $i - 1$ consecutive pedestrian VAMs being lost in the wireless channel, and having an ith VAM transmission success has probability $p(\Lambda(\omega))[1 - p(\Lambda(\omega))]^{i-1}$. Therefore, the average IPG is computed as:

$$\mathbb{E}[\text{pIPG}] = \sum_{i=1}^{\infty} \frac{i}{n_p \lambda(\omega)} \, p(\Lambda(\omega))[1 - p(\Lambda(\omega))]^{i-1}$$

$$= \frac{1}{n_p \lambda(\omega) p(\Lambda(\omega))} \quad (31)$$

with $\frac{i}{n_p \lambda(\omega)}$ the time ellapsed between first and i$^{\text{th}}$ VAM sent to the channel. $\qquad \square$

To find the optimum sampling rate we check which pedestrian VAM rate $\lambda(\omega)$ minimizes the average pIPG.

Problem 1 (VAM pIPG minimization). *Given n_b bikes with average VAM rate λ_b, n_c cars with average VAM rate λ_c, and n_p pedestrians; solve*

$$\min_{\omega} \quad \mathbb{E}[\text{pIPG}] \qquad (32)$$

$$s.t.: \quad \omega \leq \omega_{\max} \qquad (33)$$

with $\omega_{\max}$ the maximum positioning sampling frequency.

To solve Problem 1 we take the derivative of (30) denoting $\lambda = \lambda(\omega)$, i.e.:

$$\frac{d}{d\lambda}\mathbb{E}[\text{pIPG}] = \frac{-1}{n_p (\lambda p(\lambda))^2} \left[p(\lambda) + \lambda p'(\lambda) \right] \qquad (34)$$

with $p(\lambda) = p(\Lambda(\omega))$ to ease notation given the dependancy of $\Lambda(\omega)$ on $\lambda(\omega)$ – see (29).

From (34) we see that a local optimum is found at $\lambda_0 : p(\lambda_0) = -\lambda_0 p'(\lambda_0)$. We know the PDR $p(\lambda) \in [0, 1]$ is a monotonically decreasing function on λ – i.e. the transmission success probability decreases as the rate λ increases – and $p(0) = 1$. But $p(\lambda)$ depends on the used radio technology – e.g. NR or 802.11p –, and it may be that λ_0 has multiplicity greater than one, i.e. that there are multiple local minimums.

We take the second derivative of the average pIPG to gain further understanding

$$\frac{d^2}{d\lambda^2}\mathbb{E}[\text{pIPG}] = \frac{2 \left[p(\lambda) + \lambda p'(\lambda) \right]^2}{n \left(\lambda p(\lambda) \right)^3} - \frac{2 p'(\lambda) + n \lambda p''(\lambda)}{n(\lambda p(\lambda))^2} \qquad (35)$$

For we do not know how the second derivate of the PDR is, we cannot tell whether $p''(\lambda) > 0, \forall \lambda$ to fully determine the convexity of $\frac{d^2}{d\lambda^2}\mathbb{E}[\text{pIPG}]$, hence, to conclude that λ_0 has multiplicity one and there exists an unique global minimum.

To gain further understanding on the second derivative of the expected pIPG, in the next section we study $p(\lambda)$ for 802.11p, and solve Problem 1. Towards the end of the next section we also explain how to adapt the proposed 802.11p solution to other technologies as 802.11bd and C-V2X.

6.1 802.11p Pedestrian IPG Minimization

In this section we resort to the PDR expression $p(\Lambda(\omega))$ of the 802.11p node model in [18, §III-A], and find the optimal ω to solve Problem 1. The node model in [18] takes two assumptions:

A1) 802.11p devices generate packets (VAMs/CAMs) at a Poissonian rate; and

A2) 802.11p devices have an homogeneous VAM/CAM rate that we obtain as an equal split of the aggregate rate in (29) – i.e. each device has an average rate $\Lambda(\omega)/n$.

Both assumptions are taken for the sake of analytical tractability. Although assumption A1) does not hold – see [27, Figure B.4] –, it serves us to take a conservative approximation on the optimum ω due to the long tail of the exponential inter-arrival times of Poissonian processes. Assumption A2) is neither realistic for cars generate CAMs at a higher rate than pedestrian VAMs. However, assumptions A1) and A2) hold upon sufficiently large VAMs and CAMs in 802.11p, for the aggregation of arrival processes results into a Poissonian arrival process according to the Palm-Khintchine theorem [28]. Nevertheless, later in §7.3 we investigate scenarios with small/large number of VAM/CAMs to highlight the drawback/advantages of assumptions A1) and A2).

The node model obtains a recurrence expression [18, (15)] for the probability τ of an 802.11p node transmitting at a virtual time slot that consists of *an idle back-off slot, or an idle back-off slot followed by a transmission* – see [18, §II-C]. Specifically, the PDR is obtained as

$$p(\Lambda(\omega)) = (1 - \tau)^{n-1} \qquad (36)$$

with τ depending on the aggrefated rate of VAMs and CAMs $\Lambda(\omega)$.

While using the expressions of [18] we found a typo in the manuscript that we correct to obtain the PDR term τ – see Appendix C for further details.

For τ does not have either a closed-form expression – it is found through fixed-point iteration [18, §III-B] – we cannot either conclude whether the local optimum for the average pIPG near $\lambda = 0$ is a global optimum. However, we see through numerical inspection that the PDR (36) has two concave regions, hence, two candidate global minimums.

In Fig. 6 we depict how the pedestrian VAM rate λ influences the average pIPG as the pedestrians, bikes and cars increase. Results are obtained plugging the PDR expression from the node model (36) into the average pIPG expression in (30).

Fig. 6 evidences the existence of two concave regions. Consequently, gradient descends from $\lambda = 0$ leads to a global optimum only in certain scenarios – e.g. for the 24 bikes & cars and 16 pedestrians in Fig. 6. In other scenarios, gradient descends starting from $\lambda = 0$ get stuck in the left local optimum, and do not reach the global minimum at the right – e.g. for the scenario without bikes and cars with 16 pedestrians in Fig. 6.

Motivated by the numerical evidences of the average pIPG – see Fig. 6 –, we conjecture that it is possible to solve Problem 1. Specifically, we propose Algorithm 1 to obtain the sampling rate ω that minimizes the average pedestrian IPG.
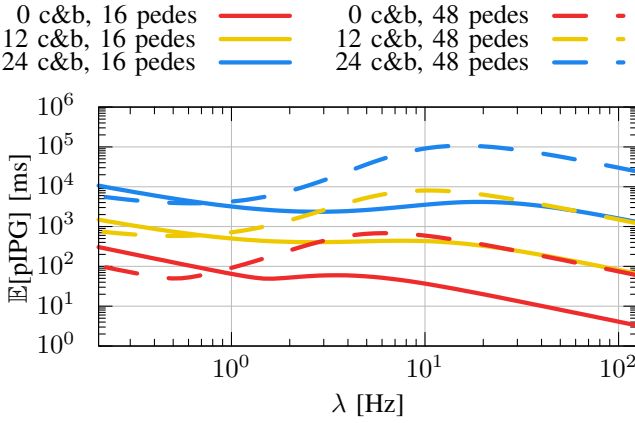
0 c&b, 16 pedes	———	0 c&b, 48 pedes	— -
12 c&b, 16 pedes	———	12 c&b, 48 pedes	— -
24 c&b, 16 pedes	———	24 c&b, 48 pedes	— -

Fig. 6: Average pIPG vs. the pedestrian VAM rate for densities $\mu = 0.01 \, \text{ped/m}^2$ (16 ped), $\mu = 0.03 \, \text{ped/m}^2$ (32 ped), and equally increasing amount of cars and bikes (c&b) $n_b = n_v$. CAM/VAM rates are $\lambda_c = 3$ and $\lambda_b = 1 \, \text{Hz}$.

Algorithm 1 802.11p pedestrian sampling rate search

Input: $n, n_p, \Lambda_b, \Lambda_v, \{\lambda_\theta(\omega_i)\}_{i=0}^{N}$
Output: ω^*
1: $\lambda = \lambda_{\max}$
2: $\text{pIPG}_0 = -10$
   $\qquad\qquad\qquad\qquad\qquad \triangleright$ Invoke Algorithm 2 as pIPG()
3: **while** $\text{pIPG}(n, n_p, \Lambda_b, \Lambda_v, \lambda) > \text{pIPG}_0$ **do**
4: $\quad \text{pIPG}_0 = \text{pIPG}(n, n_p, \Lambda_b, \Lambda_v, \lambda)$
5: $\quad \lambda = \lambda + \varepsilon_\lambda$
6: **end while**
7: $\lambda_l = \text{Brent}((\lambda_{\min}, \lambda), \text{pIPG})$
8: $\lambda_r = \text{Brent}((\lambda, \lambda_{\max}), \text{pIPG})$
9: $\lambda_{\min} = \arg\min_{\lambda \in \{\lambda_l, \lambda_r\}} \{\text{pIPG}(n, n_p, \Lambda_b, \Lambda_v, \lambda)\}$
10: $\omega^* = \arg\min_\omega \{|\lambda_{\min} - \lambda_\Delta - \lambda_\sigma - \lambda_\theta(\omega)|\}$

The basic idea of Algorithm 1 is to look for the pIPG local maximum starting near large values of λ. Then, it triggers two bounded gradient descends for small and large values of λ to obtain the two local minimums shown in Fig. 6.

First, we look for the λ corresponding to the local maximum of the average pIPG – see line 3. The pIPG is obtained using Algorithm 2, which uses [18] node model fixed point iteration to find the PDR – Algorithm 2 line 2 – and return the corresponding average pIPG.

Second, we issue two bounded minimizations using the Brent method [29], [30] to the left and right of the local maximum λ. That is, we issue bounded minimization within the intervals $(\lambda_{\min}, \lambda)$ and $(\lambda, \lambda_{\max})$ to obtain the left and right local minimums λ_l, λ_r; respectively. The global minimum $\lambda_{\min}$ is obtained checking which λ_l, λ_r results into a smaller average pIPG – line 9.

Finally, we look for the pedestrian sampling rate ω resulting in a rate $\lambda = \lambda_\Delta + \lambda_\sigma + \lambda_\theta(\omega)$ that is close to $\lambda_{\min}$. In such search we leverage pre-computed estimations of $\lambda_\theta(\omega_i)$ for different sampling rates $\omega_0, \omega_i, \ldots, \omega_N$. We also resort to pre-computed estimations of $\lambda_\Delta, \lambda_\sigma$.

Note that our approach is adaptable to technologies as 802.11bd and C-V2X. First, it is necessary to obtain a closed-form expression or interpolation for the PDR $p(\Lambda(\omega))$ and

---

Algorithm 2 Average 802.11p pIPG

Input: $n, n_p, \Lambda_b, \Lambda_v$
Output: pIPG
1: $\Lambda = \Lambda_v + \Lambda_b + n_p\lambda$
   $\qquad\qquad \triangleright$ Find PDR τ using [18, (15)] fixed point iteration
2: $\tau = \text{fixed\_point\_iteration}(\tau_0 = 0, \text{rate}=\Lambda/n, \text{devices}=n)$
3: $p(\Lambda) = (1 - \tau)^{n-1}$
4: $\text{pIPG} = [n_p\lambda p(\Lambda)]^{-1}$

---

plug it into Algorithm 2 line 3. Then, Algorithm 1 should be adapted to consider the multiplicity of the solution to $\frac{d}{d\lambda}\mathbb{E}[\text{pIPG}] = 0$ in the considered technology – e.g. 802.11bd. If the multiplicity is one, a gradient descend on λ would suffice, otherwise, it is necessary to study the shape of $\mathbb{E}[\text{pIPG}]$ vs λ (see Fig. 8). For example, if $\frac{d}{d\lambda}\mathbb{E}[\text{pIPG}] = 0$ has multiplicity three, it is necessary to issue three Brent searches (rather than the two issued in Algorithm 1 for 802.11p) and compare which of the three solutions yields the minimum $\mathbb{E}[\text{pIPG}]$.

7 RESULTS

In this section we: validate the pedestrian VAM characterization (§7.1); and evaluate Algorithm 1 through numerical and simulation experiments (§7.2 and 7.3, respectively).

7.1 Pedestrian VAM Rate Validation

In this section we validate whether the estimations specified in §3–5 for $\lambda_\Delta, \lambda_\sigma, \lambda_\theta$ hold. For the VAMs due to changes of position λ_Δ we assume a constant speed for its approximation, hence, we resort to the expression in (1). In the case of the VAMs due to speed changes we leverage Lemma 1 using an ODE warmup of 10 sec – i.e. we take $\lambda_\sigma \simeq \lambda_\sigma(i_0)$ with $i_0 = 10$. The VAMs due to orientation changes are approximatted using the average expression from Lemma 4.

We consider that pedestrians have an average speed of $\sigma = 1.34 \, \text{m/sec}$ and walk along the two sidewalks of a street of $2 \, \text{km}$. We consider three different densities of $\mu = 0.13, 0.2505, 0.4515 \, \text{ped/m}^2$ and test different positioning sampling rates in the range $10^{-2} \, \text{Hz} \leq \omega \leq \omega_{\max}$. In particular, we choose $\omega_{\max} = 10 \, \text{Hz}$ because (i) that is the maximum sampling rate of high precision commercial devices [32, 12]; (ii) we observe empirically that pedestrian VAM rates do not increase with $\omega \geq 10 \, \text{Hz}$; and ($iii$) ETSI [7, 6.2] imposes a minimum positioning sampling rate of $10 \, \text{Hz}$. Pedestrians travel in opposite directions in both sidewalks, hence leading to situations in which pedestrians have to avoid people coming towards them in the opposite direction.

Fig. 7 shows how VAM rates increase with the positioning sampling rate ω. Clearly, having higher sampling rates increases the chances of detecting changes of position, speed, and orientation – thus increasing the corresponding VAM rates $\lambda_\Delta, \lambda_\sigma, \lambda_\theta$. While the VAM rate is monotonically increasing on ω for speed and orientation changes – see Fig. 7 middle and right –, the VAM rate due to changes of position present notorious oscillations when $\omega \in [10^{-1}, 10^0]$ – see Fig. 7 left. The oscillating behaviour is inline with the saw-teeth curves already presented in Fig. 2, and Vadere
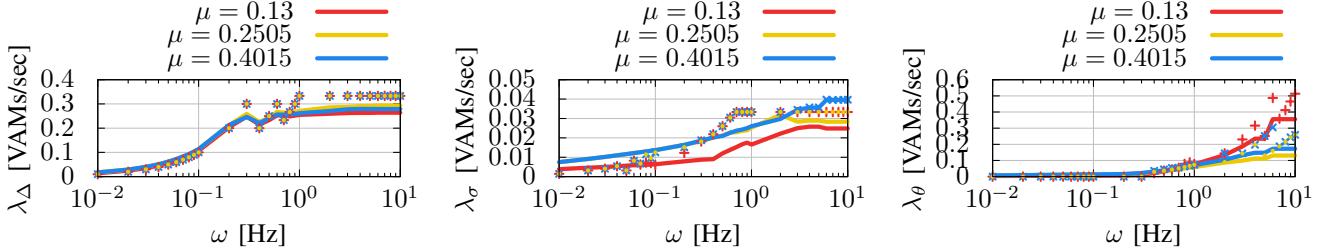
Fig. 7: Average VAM rate due to changes of position λ_Δ, change of speed λ_σ and change of orientation λ_θ. Lines represent results obtained through Vadere [31] simulations and markers represent results from our theoretical approximations §3–5.

TABLE 2: VAM approximations' (§3–5) errors.

		Error Percentile $|\lambda_* - \hat\lambda_*|$			
Density	VAM Trigger	25	50	75	100
$\mu = 0.13$	Distance λ_Δ	0.006	0.018	0.070	0.078
$\mu = 0.2505$	Distance λ_Δ	0.012	0.026	0.040	0.062
$\mu = 0.4015$	Distance λ_Δ	0.012	0.021	0.054	0.072
$\mu = 0.13$	Speed λ_σ	0.002	0.008	0.013	0.000
$\mu = 0.2505$	Speed λ_σ	0.004	0.005	0.006	0.010
$\mu = 0.4015$	Speed λ_σ	0.002	0.006	0.008	0.000
$\mu = 0.13$	Orientation λ_θ	0.005	0.006	0.016	0.157
$\mu = 0.2505$	Orientation λ_θ	0.008	0.013	0.020	0.128
$\mu = 0.4015$	Orientation λ_θ	0.007	0.012	0.022	0.132

simulations – points in Fig. 7 – are inline with the modelled oscillating behaviour (1) for λ_Δ.

Regardless the event triggering the VAMs, Fig. 7 evidences that the VAM rates stabilize for large enough sampling rates ω. Specifically, λ_Δ stabilizes for $\omega \geq 1\,\text{Hz}$; λ_σ around for $\omega \geq 3\,\text{Hz}$; and λ_θ at sampling rates $\omega \geq 5\,\text{Hz}$. Additionally, we observe that the stabilization of λ_σ (speed changes) depends on the pedestrian density μ, for it is not as easy to e.g. start running when streets are empty than when they are full.

Lastly, it is worth remarking that our analytical approximations for $\lambda_\Delta, \lambda_\sigma, \lambda_\theta$ stay close to the results obtained through simulation – see Fig. 7 and Table 2. Indeed, our analytical approximations are conservative for sampling rates $\omega > 10^{-1}\,\text{Hz}$, i.e. simulations yield smaller VAM rates. In other words, our analytical expressions for $\lambda_\Delta, \lambda_\sigma, \lambda_\theta$ are conservative, yet accurate if the positioning is checked — at least — every 10 sec.

7.2 Numerical Results

In this section we validate the applicability of Algorithm 1 through numerical evaluation. Specifically, we evaluate the performance of Algorithm 1 using the 802.11p node model [18], i.e. we consider that devices obey the exponential assumptions A1) and A2) in §6.1.

In the experiments we consider an increasing amount of bikes $n_b = 6, 12, 24$ in a street of $2\,\text{km}$ — as in §7.1. Each bike as an average VAM rate of $\lambda_b = 1\,\text{Hz}$ [33]. Similarly, we consider an increasing amount of cars $n_c = 6, 12, 24$ in the $2\,\text{km}$ street, each with an average CAM rate of $\lambda_c = 3\,\text{Hz}$. Note that the Decentralized Congestion Control (DCC) clips the CAM rate to at most $3\,\text{Hz}$ [34].

Pedestrians VAM rate $\lambda(\omega)$ will depend on the optimal positioning sampling frequency ω^* found by Algorithm 1 based on the pedestrian density μ in the sidewalks – see Fig. 7. For we consider the densities in §7.1, i.e. densities of $\mu = 0.13, 0.2505, 0.4015\,\text{ped}/\text{m}^2$ that correspond to $n_p = 16, 32, 48$ pedestrians in the considered $2\,\text{km}$ street. Given the pedestrian VAM rate characterizations from §3–5, we know that the maximum VAM rate remains below $1\,\text{Hz}$ because $\lambda_\Delta + \lambda_\sigma + \lambda_\theta < 1\,\text{Hz}$ at the maximum positioning sampling frequency $\omega_{\max} = 10\,\text{Hz}$ – see Fig. 7 results.

Fig. 8 illustrates the two local minimums that the average pIPG presents as the pedestrian VAM rate λ varies in the following scenarios: (i) only pedestrians Fig. 8 (left); (ii) 32 pedestrians with only bikes Fig. 8 (mid-left); (iii) 32 pedestrians with only cars Fig. 8 (mid-right); and (iv) 32 pedestrians with cars and bikes Fig. 8 (right). The gray areas highlight the minimum and maximum VAM rate generated by pedestrians due to the maximum positioning sampling rate limitation of $\omega_{\max} = 10\,\text{Hz}$.

If only pedestrians are present in the street, having more pedestrians leads to a smaller average pIPG — see Fig. 8 (left). Clearly, more pedestrians lead to more VAMs, hence to smaller time ellapsed between two pedestrian VAMs. However, the increase of bikes or/and cars — see Fig. 8 (mid-left) to Fig. 8 (right) — lead to a higher average pIPG. High number of bikes and cars result into more packet collisions in the 802.11p channel, hence pedestrian VAMs are prone to fail and the average pIPG increases.

Motivated by the insights of Fig. 8, we evaluate Algorithm 1 in scenarios with: (i) increasing number of bikes Fig. 9 (left); (ii) cars Fig. 9 (middle); and (iii) increasing number of bikes and cars Fig. 9 (right). Namely, we compare the average pIPG in the 802.11p channel using ETSI positioning sampling frequency $\omega = 10\,\text{Hz}$, and the optimal sampling frequency ω^* that Algorithm 1 yields. Note that ETSI [7] imposes $\omega \geq 10\,\text{Hz}$, however high precision commercial GPS devices [32] offer maximum rates of $10\,\text{Hz}$; thus setting ETSI positioning sampling rate to $\omega = 10\,\text{Hz}$.

Fig. 9 numerical results evidence that the optimal positioning sampling rate ω^* matches ETSI sampling rate $\omega = 10\,\text{Hz}$ in scenarios with only 16 pedestrians, regardless the number of cars and bikes. Hence, ETSI positioning sampling rate is clearly optimal upon scenarios with low pedestrian densities.

We now check what happens in scenarios with 32 and 48 pedestrians. If only bikes are present — see Fig. 9 (left) — the optimal positioning sampling rate ω^* always remains below ETSI sampling rate $\omega = 10\,\text{Hz}$. However, upon the presence of cars — see Fig. 9 (middle) and Fig. 9 (right) — the optimal
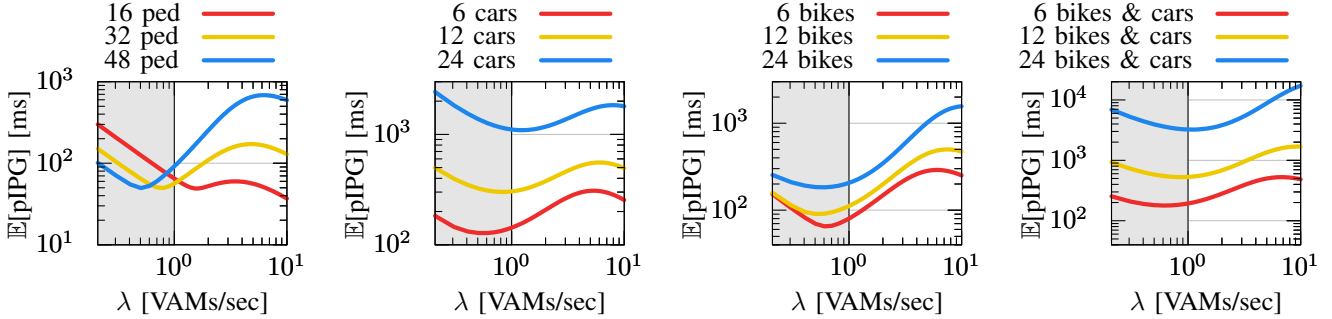
Fig. 8: Average pIPG (y-axis) vs. their VAM rate (x-axis) in a sub-urban scenario. In the left we consider only pedestrians. The remaining scenarios consider 32 pedestrians and bikes (mid-left) or cars (mid-right). The scenario on the right consider 32 pedestrians with N bikes and N cars. Gray areas highlight the pedestrian VAM rate range.
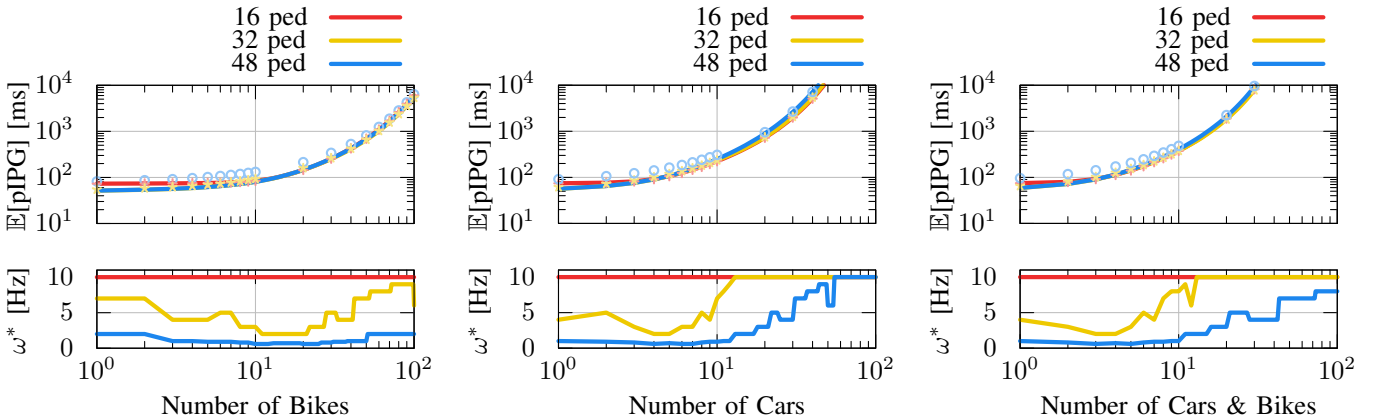

Fig. 9: Optimal positioning sampling frequency ω^* (bottom) and their average pedestrians IPG (top). Markers on top correspond to the pedestrian IPG experienced using ETSI [7] sampling frequency $\omega = 10$ Hz. Results are obtained using [18] 802.11p node model (bottom) and Algorithm 1.

positioning sampling rate ω^* increases with the number of cars. Given the high CAM rate of cars $\lambda_c = 3$ Hz, large number of vehicles lead to more 802.11p collisions and it is necessary to send/generate more pedestrian VAMs (using higher rates ω^*) to guarantee their delivery.

However, numerical results highlight that the optimal sampling frequency ω^* increases at a lower pace upon high density of pedestrians. For example, Fig. 9 (right) shows how the optimal sampling rate ω^* remains below 10 Hz if 48 pedestrians are in the street, regardless the number of cars & bikes. While the optimal sampling rate reaches ETSI sampling rate $\omega = 10$ Hz with just 10 cars & bikes.

Finally, the numerical results from Fig. 9 evidence how ETSI (markers) results into worse pIPG than using the optimal sampling rate ω^* obtained through Algorithm 1 (lines).

7.3 Simulation Results

In this section we evaluate the performance of Algorithm 1 in simulated scenarios. That is, rather than using the 802.11p node model [18], we resort to a vehicular simulation stack to test the performance of the pedestrian VAMs using the optimal positioning sampling frequencies found in §7.2.

We evaluate the performance of ETSI positioning sampling frequency $\omega = 10$ Hz against the optimal sampling

rate ω^* found in Algorithm 1. The scenario considered is the same one from §7.1 and 7.2, i.e. a 2 km street with two sidewalks with pedestrian and cycle lanes separated by a two-lane road. In the simulations we consider 48 pedestrians sharing the 802.11p wireless medium with 0,6,12,24, and 48 cars & bikes sending CAMs/VAMs.

The simulation setup we use is Artery [19], which implements the ETSI ITS protocol stack trough its Vanetza component. Artery uses Veins [20] to implement 802.11p. The movement of pedestrians, cyclists and vehicles is controlled by SUMO [21]. We implemented a VRU awareness basic service (VBS) following the triggering rules in [7] and took measurements for 60 seconds after warm-up periods of 100 seconds. For each simulation we perform five repetitions. The simulation parameters are described in Table 3.

To compare the performance of a VBS using the positioning sampling rate ω^* of Algorithm 1, we consider the following metrics:

- *Inter-generation gaps (IGG):* the time between two consecutive pedestrian VAM generations (measured at the transmitting node).
- *Pedestrian Inter-packet gaps (pIPG):* the time between the reception of VAMs from *any* pedestrian (measured at receiving nodes — vehicles and other VRUs).
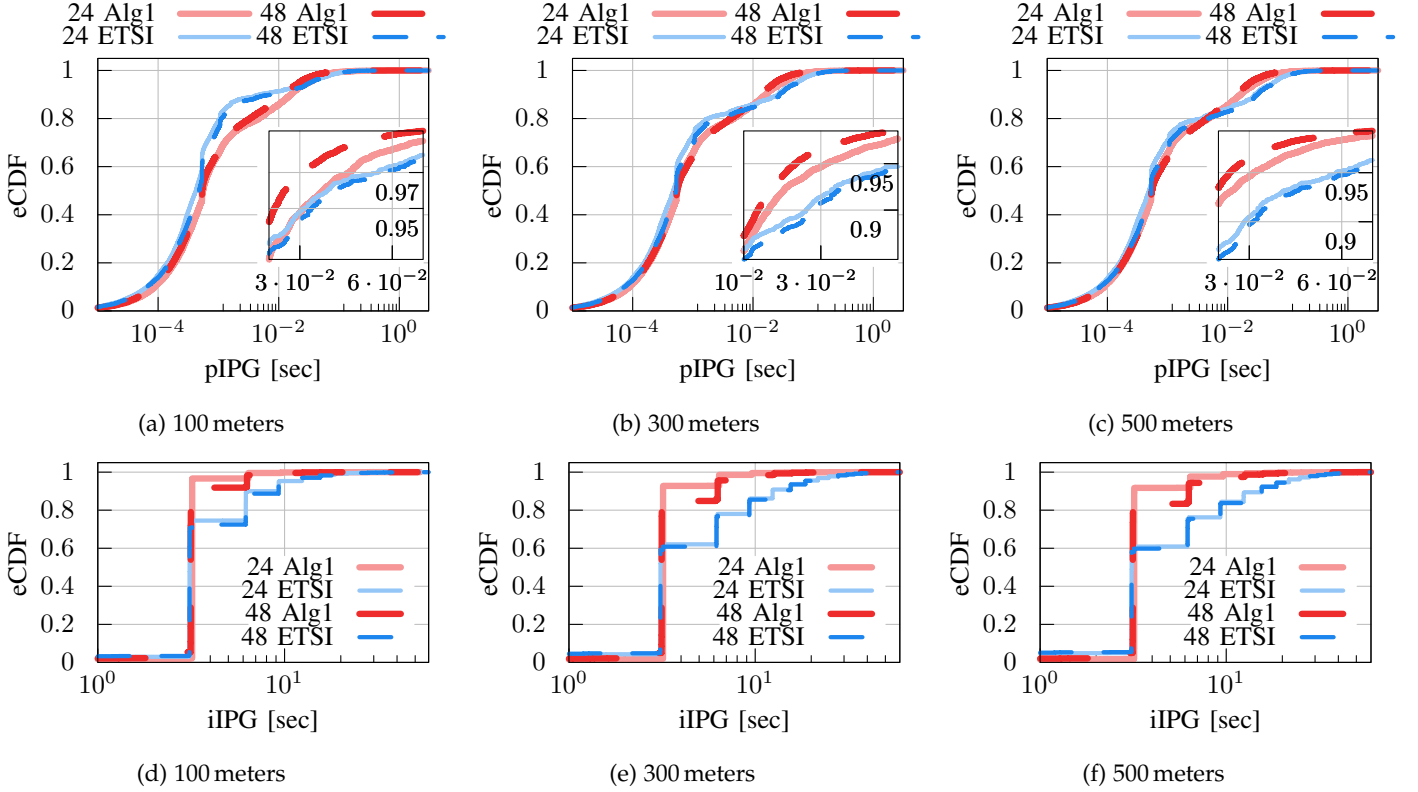- *Individual Inter-packet gaps (iIPG):* the time between the

Fig. 10: pIPG (top) and iIPG (down) empirical CDF (eCDF) for pedestrians at different distances using Artery Veins [20] 802.11p stack. We compare ETSI positioning sampling rate [7] (blue) against the Algorithm 1 (red) in scenarios with: 48 pedestrians and 24 bikes & vehicles (continuous), and 48 pedestrians with 48 bikes & vehicles (dashed). Optimal sampling rates are $\omega = 5$ Hz and $\omega = 7$ Hz for 24 and 48 bikes & vehicles, respectively.

TABLE 3: Simulation Parameters

Parameter	Values
Access Layer protocol	ITS-G5 (IEEE 802.11p)
Channel bandwidth	10 MHz at 5.9 GHz
Data rate	6 Mbit/s
Pedestrian Transmit power	16 mW
Bikes/Cars Transmit power	20 mW
Path loss model	Two-Ray interference model
VAM generation frequency	0.2–10 Hz (ETSI VAM [7])
CAM generation frequency	1–10 Hz (ETSI CAM [35])
Max. pedestrian velocity	5 km/h
Max. bicycle velocity	25 km/h
Max. vehicle velocity	60 km/h

reception of two VAMs from *one* pedestrian (measured at the receiving nodes).

- *Packet Delivery Ratio (PDR):* the ratio between generated messages and successful receptions by neighbors in an area.

Inline with §7.1, throughout the simulations we observe that pedestrians keep their VAM rate λ below 1 Hz. Thus, DCC congestion control is not triggered for it acts upon rates exceeding ~ 3 Hz [34]. Consequently, there exists the need of reducing the congestion with other mechanisms as the proposed search of an optimal positioning sampling rate ω^*.

Table 4 shows the average IGGs, iIPGs, pIPG, and PDRs for different scenarios, starting from 48 pedestrians and no

bicycles or vehicles (P-B-V 48-0-0), up to scenarios with 24 bicycles and 24 vehicles (P-B-V 48-24-24). We compare the iIPG achieved by the ETSI parameters ($\omega = 10$ Hz) and the positioning sampling obtained through Algorithm 1 – see Fig. 9. Again, note that ETSI [7] imposes $\omega \geq 10$ Hz, but high precision commercial GPS devices [32] offer maximum rates of 10 Hz. Thus, we choose ETSI positioning sampling rate $\omega = 10$ Hz.

Furthermore, it is shown from the get-go that the optimal values for ω outperform the ETSI scheme significantly, since neighbors hear from pedestrians between 0.2 and 1.17 s more frequently. It is possible to compare the intended update rate from pedestrians (IGG) and the actual result in iIPG. The table shows that optimal values for ω take advantage of the space left by bicycles and vehicles more efficiently, i.e., practically all of the information intended to reach neighboring nodes is received, while the ETSI schemes loses around 30% of the messages.

For the scenarios with fewer bicycles and cars (48-0-0, 48-6-6), ETSI achieves lower values for pIPG than Algorithm 1. This is due to the fact that assumptions A1) and A2) do not hold, and the objective PDR for Algorithm 1 is not correct. However, in scenarios with more bicycles and cars (48-24-44, 48-48-46), Palm-Khintchine's theorem [28] hold, which is reflected in the PDR input for Algorithm 1 and thus average pIPG is significantly lower. Nevertheless, even if ETSI has better average pIPG in some scenarios, its values for iIPG and PDR are always outperformed by Algorithm 1. The

TABLE 4: Average IGG, iIPG, pIPG and PDR at distances $\leq 100\,\text{m}$ with vaying Pedestrians (P), Bikes (B), and Cars (C). Simulations use Artery Veins [20] 802.11p stack, and we compare ETSI positioning sampling rate [7] against Algorithm 1.

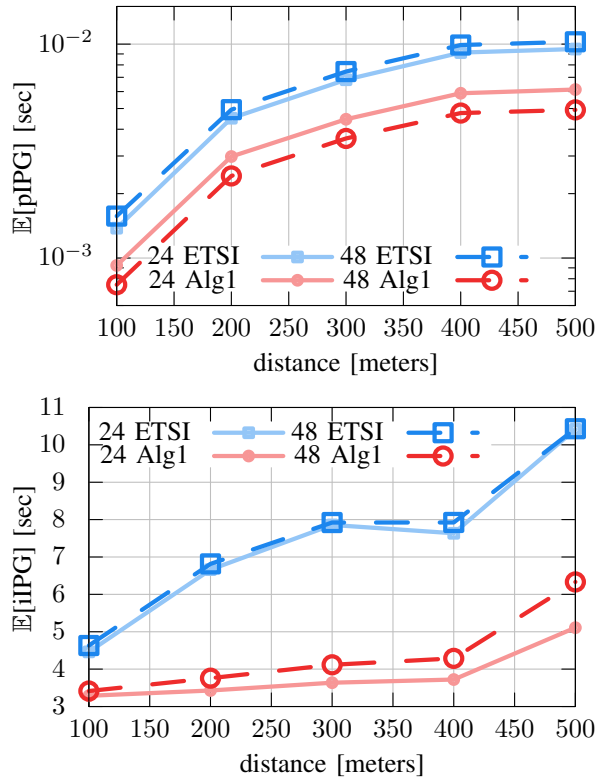| P-B-C	ETSI					Algorithm 1				
	ω	IGG	iIPG	pIPG	PDR	ω	IGG	iIPG	pIPG	PDR
48-0-0	10 Hz	3.078 sec	4.227 sec	0.0012 sec	0.7282	1 Hz	3.984 sec	4.021 sec	0.0046 sec	0.9908
48-6-6	10 Hz	3.053 sec	4.256 sec	0.0012 sec	0.7174	0.8 Hz	3.728 sec	3.759 sec	0.0058 sec	0.9916
48-12-12	10 Hz	3.054 sec	4.299 sec	0.0012 sec	0.7104	2 Hz	3.470 sec	3.496 sec	0.0022 sec	0.9925
48-24-24	10 Hz	3.055 sec	4.461 sec	0.0014 sec	0.6826	5 Hz	3.158 sec	3.287 sec	0.0009 sec	0.9618
48-48-48	10 Hz	3.056 sec	4.431 sec	0.0016 sec	0.6569	7 Hz	3.103 sec	3.415 sec	0.0007 sec	0.9098

Fig. 11: Average pIPG (top) and iIPG (bottom) of pedestrians at different distances using Artery Veins [20] 802.11p stack. We compare ETSI positioning sampling rate [7] (blue) against the Algorithm 1 (red) in scenarios with: 48 pedestrians and 24 bikes & vehicles (continuous), and 48 pedestrians with 48 bikes & vehicles (dashed). Optimal sampling rates are $\omega = 5\,\text{Hz}$ and $\omega = 7\,\text{Hz}$ for 24 and 48 bikes & vehicles, respectively.

lower average values for iIPG mean that pedestrians using Algorithm 1 are tracked better and more often than those using the ETSI mechanism.

The PDR values from Table 4 have implications in other performance metrics such as energy consumption. Every message that is transmitted consumes a certain amount of energy which can be obtained by multiplying the transmission power (16 mW) and the time it takes for a transmission to occur (i.e., 467.424 μs for a VAM). Schemes using the optimal ω transmit between 3 and 30% fewer messages than the ETSI scheme, which then wastes around 30% of its transmission power consumption in colliding messages. All in all, optimal ω schemes is more efficient in resource usage, from energy to medium.

Fig. 10 shows the effect of ω on pIPG and iIPG. The upper part of the figure shows pIPG results for ETSI VAM and Algorithm 1. While lines for ETSI and Algorithm 1 overlap, a zoom into important regions is also provided. There, it is noticeable that pIPG values for Algorithm 1 stay lower than those for ETSI and this difference increases with distance. The results for ETSI show that extremely large values for pIPG occur in all distances (i.e., its distribution has a longer tail).

Moreover, the lower part of Fig. 10 shows results for iIPG. Here, results show that Algorithm 1 has better iIPGs in all percentiles, while the ETSI mechanism has a significant number of neighbors waiting more than 10 seconds between updates. Scenarios using the calculated optimal ω are more reliable, and deliver most updates at rates closer to the IGGs from Table 4. While pIPG is a measure of efficient channel utilization, iIPG can be translated to a safety metric: *awareness*. In safety terms, Algorithm 1 outperforms ETSI VAM significantly by allowing nodes keep better track of pedestrians by minimizing the time between two successful updates.

Fig. 11 shows results for pIPG and iIPG over the distance. Once again, in crowded scenarios, Algorithm 1 manages to minimize pIPG. Regarding awareness, iIPG values stay stable through longer distances when optimal values for ω are used. Receptions at longer distances are affected by attenuation and phenomena such as hidden nodes. However, Akgorithm 1 manages to stay stable up to 400 m. These results validate the analysis shown in §7, and emphasizes the importance of the optimal sampling rate to increase VRU safety.

Results from the experimental evaluation of the effect of optimal sampling rates for VAMs confirm what the analytical results proposed. First, given that the dynamics of a pedestrian are different to those of a vehicle, positioning sampling can be less aggressive and still react to changes in speed and orientation. Second, that even if less aggressive schemes are used and generation frequencies are lowered, messages are received more frequently with less greedy sampling rates. Finally, optimal values for ω affect performance favorably in the most important metric: awareness. Other stations are able to see pedestrians more frequently and at longer distances, a significant improvement from the standardized scheme.

8 RELATED WORK

The dissemination of awareness messages, e.g., VAMs and CAMs, is one of the main topics in the study of V2X and P2X

communications. Additionally, it is necessary to comprehend the wireless channel access to analyze the performance of awareness services. Existing work in the literature has analyzed the aforementioned topics, and their results relate to the research of the present manuscript.

Wireless Channel Access. Cooperative awareness in V2X/P2X communications use Direct Short Range Communication technologies (DSRC) as 802.11p/bd, and C-V2X to deliver VAMs/CAMs. The literature has already analyzed the differences between both C-V2X and DSRC technologies through simulation in the physical layer [36], and field tests [37]. Moreover, the research community has also studied the access layer of both DSRC and C-V2X technologies. In particular, works as [38] study how persistent scheduling impacts the Age of Information (AoI) in the NR sidelink, while others as [18] focus on the impact of 802.11p congestion on the AoI when DCC does not apply (as in the case of pedestrian VAMs). Moreover, works as [14] propose mechanisms to improve the DCC efficiency, and assess its performance through simulation [34].

CAMs. Given the rise of autonomous vehicles, the literature has also studied recently the performance of CAMs. Namely, works as [39] model how CAMs are generated depending on kinematic triggers (e.g. change of position), while other works focus on how performance evaluation on either NR sidelink channels [40] and 802.11p channels [13]. On top, researchers have also come up with mechanisms to: adapt the CAM generation in windy scenarios [41]; anticipate to dangerous events through Machine Learning [42]; or combine sensing information from vehicles, pedestrians and infrastructure to enhance vehicle awareness [9].

VRUs and VAMs. Works as [5] state potential of sending awareness messages concerning pedestrians/VRUs in future mobility scenarios – i.e. VAMs. Either by assessing its performance with onboard units [43] or roadside cameras [8], results show the potential of VAMs to prevent accidents. In particular, the research community has assessed the awareness performance of ETSI VA [7] in LTE [10], 802.11p/bd and C-V2X PC5 [12]. Moreover, the literature has also studied how to increase the awareness level of ETSI VAMs using passive perception – e.g. vehicle camera detecting a pedestrian – together with the active transmission of VAMs [9], [44]. Furthermore, works as [15] study how VRU clusters decrease the collision of VAMs in the wireless channel upon high density of pedestrians.

Despite the existing literature on VAM/CAMs, to the best of our knowledge there is no analysis on how decreasing the positioning sampling rate may enhance the awareness of ETSI VAMs coming from pedestrians. Our work aims to fill such a gap (*i*) with a detailed characterization of the pedestrian VAMs through the well-known GNM mobility model [23]; and (*ii*) an optimization problem that minimizes the time between pedestrian VAMs through adequate election of the positioning sampling rate.

9 CONCLUSION AND FUTURE WORK

In this work we study how to improve the delivery of pedestrian VAMs through optimal positioning sampling. We characterize how the positioning sampling rate impacts the rate at which VAMs are generated when pedestrians change

their: position, speed, and orientation. Simulations prove the validity of our characterization, which we leverage to design an algorithm that finds the optimal positioning sampling rate in 802.11p channels. Results show that our algorithm finds smaller positioning sampling rates than the proposed by ETSI ($\omega = 10\,\text{Hz}$) to check if a VAM must be generated. Moreover, simulations with 24 and 48 cars & bikes evidence that decreasing the positioning sampling rate by a 50% and 30%, respectively, results into reducing the inter packet gap of pedestrian VAMs and an increasing the VAM delivery ratio. Hence, the optimal positioning sampling rates found by our algorithm result into battery savings and higher pedestrian safety.

In future work we plan to extend our simulation campaign to even denser scenarios, and investigate how the optimal positioning sampling rate varies using other wireless technologies as the NR sidelink or 802.11bd. Additionally, we aim to study: (*i*) other VRU profiles (e.g. bikes and scooters); (*ii*) the impact of the pedestrians' height and their ongoing activity (e.g. listening to music) on the VAM rate; (*iii*) whether intention sharing alters the VAM rate; and (*iv*) how VRU clustering may allow reducing the positioning sampling rate, yet keeping the VAM delivery ratio.

REFERENCES

[1] World Health Organization (WHO). (2022) Road traffic injuries. [Online]. Available: https://www.who.int/news-room/fact-sheets/detail/road-traffic-injuries

[2] European Commission (EC). (2023) Road safety in the EU: fatalities below pre-pandemic levels but progress remains too slow. [Online]. Available: https://ec.europa.eu/commission/presscorner/detail/en/ip_23_953

[3] ——, "Towards a European road safety area: policy orientations on road safety 2011-2020," July 2010.

[4] United Nations, Department of Economic and Social Affairs - Sustainable Development, "Transforming our world: the 2030 agenda for sustainable development," p. 16301, 2015. [Online]. Available: https://sdgs.un.org/2030agenda

[5] M. Bied, B. Bruno, and A. Vinel, "Autonomous Vehicles as Social Agents: Vehicle to Pedestrian Communication from V2X, HCI and HRI Perspectives," *Submitted*, 2024.

[6] SAE, "Vulnerable Road User Safety Message Minimum Performance Requirements," SAE International, Standard, Mar. 2017.

[7] ETSI, "Intelligent Transport Systems (ITS); Vulnerable Road Users (VRU) awareness; Part 3: Specification of VRU awareness basic service; Release 2," European Telecommunications Standards Institute (ETSI), Technical Specification (TS) 03-300-3 v2.1.1, 11 2020.

[8] M. Islam, M. Rahman, M. Chowdhury, G. Comert, E. D. Sood, and A. Apon, "Vision-Based Personal Safety Messages (PSMs) Generation for Connected Vehicles," *IEEE Transactions on Vehicular Technology*, vol. 69, no. 9, pp. 9402–9416, 2020.

[9] S. Lobo, A. Festag, and C. Facchi, "Enhancing the Safety of Vulnerable Road Users: Messaging Protocols for V2X Communication," in *2022 IEEE 96th Vehicular Technology Conference (VTC2022-Fall)*, 2022, pp. 1–7.

[10] L. Lusvarghi, C. A. Grazia, M. Klapez, M. Casoni, and M. L. Merani, "Awareness Messages by Vulnerable Road Users and Vehicles: Field Tests via LTE-V2X," *IEEE Transactions on Intelligent Vehicles*, vol. 8, no. 10, pp. 4418–4433, 2023.

[11] C. Zhang, J. Wei, S. Qu, C. Huang, J. Dai, P. Fu, Z. Wang, and X. Li, "Implementation of a V2P-Based VRU Warning System With C-V2X Technology," *IEEE Access*, vol. 11, pp. 69 903–69 915, 2023.

[12] M. Karoui, V. Berg, and S. Mayrargue, "Assessment of V2X Communications For Enhanced Vulnerable Road Users Safety," in *2022 IEEE 95th Vehicular Technology Conference: (VTC2022-Spring)*, 2022, pp. 1–5.

[13] N. Lyamin, A. Vinel, M. Jonsson, and B. Bellalta, "Cooperative Awareness in VANETs: On ETSI EN 302 637-2 Performance," *IEEE Transactions on Vehicular Technology*, vol. 67, no. 1, pp. 17–28, 2018.

[14] O. Amador, I. Soto, M. Urueña, and M. Calderon, "GoT: Decreasing DCC Queuing for CAM Messages," *IEEE Communications Letters*, vol. 24, no. 12, pp. 2974–2978, 2020.

[15] M. Rupp and L. Wischhof, "Evaluation of the Effectiveness of Vulnerable Road User Clustering in C-V2X Systems," in *2023 IEEE International Conference on Omni-layer Intelligent Systems (COINS)*, 2023, pp. 1–5.

[16] Car 2 Car Consortium. (2020) Petition on the proposal of splitting the 5.9 GHz frequency band. [Online]. Available: https://www.car-2-car.org/press-media/press-releases/press-details?tx_news_pi1%5Baction%5D=detail&tx_news_pi1%5Bcontroller%5D=News&tx_news_pi1%5Bnews%5D=20&cHash=cbe6898f9260599d7c7e32e6b43a1760

[17] Commsignia, "Welcome to the world of Commsignia," 2022, [Online; accessed 25 July 2022]. [Online]. Available: https://www.commsignia.com/

[18] A. Baiocchi, I. Turcanu, N. Lyamin, K. Sjöberg, and A. Vinel, "Age of Information in IEEE 802.11p," in *2021 IFIP/IEEE International Symposium on Integrated Network Management (IM)*, 2021, pp. 1024–1031.

[19] R. Riebl, H. Günther, C. Facchi, and L. Wolf, "Artery: Extending Veins for VANET Applications," in *2015 International Conference on Models and Technologies for Intelligent Transportation Systems (MT-ITS)*, 2015, pp. 450–456.

[20] C. Sommer, R. German, and F. Dressler, "Bidirectionally Coupled Network and Road Traffic Simulation for Improved IVC Analysis," *IEEE Transactions on Mobile Computing*, vol. 10, no. 1, pp. 3–15, 2011.

[21] D. Krajzewicz, J. Erdmann, M. Behrisch, and L. Bieker, "Recent Development and Applications of SUMO - Simulation of Urban MObility," *International Journal On Advances in Systems and Measurements*, vol. 5, no. 3&4, pp. 128–138, December 2012.

[22] U. Weidmann, "Transporttechnik der fußgänger: transporttechnische eigenschaften des fußgängerverkehrs, literaturauswertung," *IVT Schriftenreihe*, vol. 90, 1993.

[23] F. Dietrich and G. Köster, "Gradient navigation model for pedestrian dynamics," *Phys. Rev. E*, vol. 89, p. 062801, Jun 2014. [Online]. Available: https://link.aps.org/doi/10.1103/PhysRevE.89.062801

[24] J. Dormand and P. Prince, "A family of embedded runge-kutta formulae," *Journal of Computational and Applied Mathematics*, vol. 6, no. 1, pp. 19–26, 1980. [Online]. Available: https://www.sciencedirect.com/science/article/pii/0771050X80900133

[25] A. Baddeley, I. Bárány, and R. Schneider, *Stochastic geometry: lectures given at the CIME summer school held in Martina Franca, Italy, September 13–18, 2004.* Springer, 2007.

[26] C.-S. Choi and F. Baccelli, "A Stochastic Geometry Model for Spatially Correlated Blockage in Vehicular Networks," *IEEE Internet of Things Journal*, vol. 9, no. 20, pp. 19 881–19 889, 2022.

[27] European Telecommunications Standards Institute (ETSI), "Intelligent Transport Systems (ITS); Pre-standardization study on co-channel co-existence between IEEE- and 3GPP- based ITS technologies in the 5 855 MHz - 5 925 MHz frequency band," Standard ETSI TR 103 766 - V1.1.1, September 2021.

[28] D. P. Heyman, "Stochastic models in operations research, volume I : stochastic processes and operating characteristics / Daniel P. Heyman, Matthew J. Sobel," 1982.

[29] G. E. Forsythe, M. A. Malcolm, and C. B. Moler, *Computer Methods for Mathematical Computations.* Prentice Hall Professional Technical Reference, 1977.

[30] R. P. Brent, *Algorithms for minimization without derivatives.* Courier Corporation, 2013.

[31] B. Kleinmeier, B. Zönnchen, M. Gödel, and G. Köster, "Vadere: An Open-Source Simulation Framework to Promote Interdisciplinary Understanding," *Collective Dynamics*, vol. 4, 2019.

[32] QSTARZ, "QSTARZ GT BL-818GT Quick Start Guide," 2023, [Online; accessed 30 November 2023]. [Online]. Available: https://qstarz.s3.amazonaws.com/public/BL-818GT/documents/BL-818GT_QSG_EN.PDF

[33] European Telecommunications Standards Institute (ETSI), "Intelligent Transport Systems (ITS); Decentralized congestion control mechanisms for Intelligent Transport Systems operating in the 5 GHz range; Access layer part," ETSI EN 102 687 - V1.2.1, April 2018.

[34] O. Amador, I. Soto, M. Calderón, and M. Urueña, "Experimental Evaluation of the ETSI DCC Adaptive Approach and Related Algorithms," *IEEE Access*, vol. 8, pp. 49 798–49 811, 2020.

[35] European Telecommunications Standards Institute (ETSI), "Intelligent Transport Systems (ITS); Vehicular communications; Basic set of applications; Part 2: Specification of Cooperative Awareness basic service," ETSI, Standard EN 302 637-2 - V1.4.1, April 2019.

[36] W. Anwar, N. Franchi, and G. Fettweis, "Physical Layer Evaluation of V2X Communications Technologies: 5G NR-V2X, LTE-V2X, IEEE 802.11bd, and IEEE 802.11p," in *2019 IEEE 90th Vehicular Technology Conference (VTC2019-Fall)*, 2019, pp. 1–7.

[37] E. Moradi-Pari, D. Tian, M. Bahramgiri, S. Rajab, and S. Bai, "DSRC Versus LTE-V2X: Empirical Performance Analysis of Direct Vehicular Communication Technologies," *IEEE Transactions on Intelligent Transportation Systems*, vol. 24, no. 5, pp. 4889–4903, 2023.

[38] A. Rolich, I. Turcanu, A. Vinel, and A. Baiocchi, "Impact of Persistence on the Age of Information in 5G NR-V2X Sidelink Communications," in *2023 21st Mediterranean Communication and Computer Networking Conference (MedComNet)*, 2023, pp. 15–24.

[39] R. Molina-Masegosa, M. Sepulcre, J. Gozalvez, F. Berens, and V. Martinez, "Empirical Models for the Realistic Generation of Cooperative Awareness Messages in Vehicular Networks," *IEEE Transactions on Vehicular Technology*, vol. 69, no. 5, pp. 5713–5717, 2020.

[40] C. Campolo, A. Molinaro, A. O. Berthet, and A. Vinel, "On Latency and Reliability of Road Hazard Warnings Over the Cellular V2X Sidelink Interface," *IEEE Communications Letters*, vol. 23, no. 11, pp. 2135–2138, 2019.

[41] J. Aznar-Poveda, E. Egea-López, and A.-J. García-Sánchez, "Cooperative Awareness Message Dissemination in EN 302 637-2: an Adaptation for Winding Roads," in *2020 IEEE 91st Vehicular Technology Conference (VTC2020-Spring)*, 2020, pp. 1–5.

[42] L. Lusvarghi and M. L. Merani, "Machine Learning for Disseminating Cooperative Awareness Messages in Cellular V2V Communications," *IEEE Transactions on Vehicular Technology*, vol. 71, no. 7, pp. 7890–7903, 2022.

[43] C. Zhang, J. Wei, S. Qu, C. Huang, J. Dai, P. Fu, Z. Wang, and X. Li, "Implementation of a V2P-Based VRU Warning System With C-V2X Technology," *IEEE Access*, vol. 11, pp. 69 903–69 915, 2023.

[44] P. Teixeira, S. Sargento, P. Rito, M. Luís, and F. Castro, "A Sensing, Communication and Computing Approach for Vulnerable Road Users Safety," *IEEE Access*, vol. 11, pp. 4914 – 4930, 2023.

[45] E. A. Coddington, *An introduction to ordinary differential equations.* Courier Corporation, 2012.

APPENDIX A
BOUNDING THE ORIENTATION CHANGE

To bound the orientation change $\theta(i\omega^{-1})$ in a sampling period we cannot resort to closed form solutions of the ODE system because it is not a constant coefficient system, nor a time dependant coefficient system – see [45]. That is, we cannot express (3)-(4) as a system $\dot{y}(t) = Ay(t)$ nor $\dot{y}(t) = A(t)y(t)$. Consequently we cannot use exponentiation to solve the ODE system.

To bound the orientation we take as reference the vector $(1, 0)$ as we did in §5. Hence the second coordinate is fully determined by the former and the change of orientation, i.e. $x_2(t) = x_1(t)\sin(\theta(t))$ with $x(t) = (x_1(t), x_2(t))$. Therfore, (10) simplifies to:

$$\cos(\theta(i\omega^{-1})) = (x_1(i\omega^{-1}) - x_1((i-1)\omega^{-1}))$$
$$\cdot \left[(x_1(i\omega^{-1}) - x_1((i-1)\omega^{-1}))^2\right.$$
$$\left. + (x_1(i\omega^{-1})\sin(\phi_i) - x_1((i-1)\omega^{-1})\sin(\phi_{i-1}))^2\right]^{-\frac{1}{2}}$$
$$= \frac{1}{\sqrt{1 + A^2}} \quad (37)$$

with

$$A = \frac{x_1(i\omega^{-1})\sin(\phi_i) - x_1((i-1)\omega^{-1})\sin(\phi_{i-1})}{x_1(i\omega^{-1}) - x_1((i-1)\omega^{-1})} \quad (38)$$

and $\phi_i = x_2(i\omega^{-1})/x_1(i\omega^{-1})$.

For we want to bound the orientation change – i.e. we want $\theta(i\omega^{-1}) < \epsilon$ for ϵ small enough –, we want to find a lower bound for its cosine; i.e. we want to lower bound $(1 + A^2)^{-1/2}$ in (37). However, A depends on what is the angle of the $i\omega^{-1}$ position w.r.t the horizontal, which relates to the angle shift $\theta(i\omega^{-1})$ we are looking for. Such angle depends on the initial setting of the ODE system, namely, the pedestrian density and their starting locations. Hence, we bound (37) for every setup of the ODE.

To overcome such limitation, we approximate $\theta(i\omega^{-1})$ considering that pedestrians are distributed as a PPP, and checking their average influence on the pedestrian of interest – see §5.2.

APPENDIX B
RADIUS FOR INFLUENCE ISOLINES

As illustrated in Fig. 4, the radius for the influence isoline $h(r)s(\theta) = H$ changes with θ. Namely, the isoline H is fully determined by r, θ with the following expression [23]

$$H = \begin{cases} \dfrac{p \cdot e^{\frac{1}{(r/R_h)^2 - 1}}}{1 + e^{-(\cos(\kappa\theta) - x_0)/R_s}}, & \left(\dfrac{r}{R_h}\right)^2 < 1 \\ 0, & \left(\dfrac{r}{R_h}\right)^2 \geq 1 \end{cases} \quad (39)$$

with $p = 3.59, R_h = 0.7, \kappa = 0.6, R_s = 0.03, x_0 = 0.3$ [23].

Hence, it is possible to obtain to reverse the above equation to know the isoline radius r w.r.t the angle θ and isoline value H:

$$r(\theta, H) = R_h \sqrt{1 + \frac{1}{\log\left(\frac{H}{p}\left(1 + e^{-(\cos(\kappa\theta) - x_0)/R_s}\right)\right)}} \quad (40)$$

if $1/\log(\cdot) \in (-1, 0)$, and zero otherwise.

APPENDIX C
CORRECTION IN 802.11P NODE MODEL

According to [18], the PDR depends on the transmission probability τ of an 802.11p node – see [18, (15)]. τ depends on the probability of having zero packets in the queue of the 802.11p device π_0. Such probability π_0 depends [18, (12)] on the Laplace transform of the time it takes to serve/send a packet, a random variable denoted as C. The service time C is defined in [18, (3)] as

$$C = \sum_{j=1}^{K} X^{(j)} + \delta + T_0 \quad (41)$$

with K *a discrete random variable uniformly distributed in the set* $\{i, \ldots, W_0\}$, and W_0 the maximum size of the 802.11p contention window.

Consequently the Laplace transform of C is obtained as

$$\mathcal{L}_C(s) = \mathbb{E}_C[e^{-sc}] = \sum_{j=1}^{W_0} \mathbb{E}_C[e^{-sc}| \, K = k]\frac{1}{W_0}$$

$$= \frac{e^{-(\delta + T_0)s}}{W_0} \sum_{k=1}^{W_0} \int_0^\infty e^{-s\sum_{j=1}^k x^{(j)}} f_{C-\delta-T_o}\left(\sum_j^k x^{(j)}\right) \, dc'$$

$$= \frac{e^{-(\delta + T_0)s}}{W_0} \sum_{k=1}^{W_0} \prod_{j=1}^k \int_0^\infty e^{-sx^{(j)}} f_X(x^{(j)}) \, dc$$

$$= \frac{e^{-(\delta + T_0)s}}{W_0} \sum_{k=1}^{W_0} \mathcal{L}_X^k(s) = \frac{e^{-(\delta + T_0)s}\left[1 - \mathcal{L}_X^{W_0 + 1}(s)\right]}{W_0\left[1 - \mathcal{L}_X(s)\right]} \quad (42)$$

with $\mathcal{L}_X(s)$ the Laplace transform of a virtual slot in 802.11p [18, (6)].

Note that (42) differs from [18, (7)] because the numerator has the Laplace transform of X to the power of W_0 rather than $W_0 + 1$. Such sublte typo in the manuscript leads to smaller PDR. That is, with our correction the model slightly increases the 802.11p PDR.

Jorge Martín Pérez is an assistant professor at the Universidad Politécnica de Madrid (UPM), Spain. He obtained a B.Sc in mathematics, and a B.Sc in computer science, both at Universidad Autónoma de Madrid (UAM) in 2016. He obtained his M.Sc. and Ph.D in Telematics from Universidad Carlos III de Madrid (UC3M) in 2017 and 2021, respectively. Jorge worked as postdoc at UC3M (until 2023) in national and EU funded projects. His research focuses in optimal resource allocation in networks.

Oscar Amador Molina is an assistant professor at Halmstad University in Sweden. He obtained a B.Sc. in Telematics Engineering at Universidad Politécnica de Durango, Mexico, in 2012, and the M.Sc. and Ph.D. degrees in Telematics Engineering at Universidad Carlos III de Madrid (UC3M), Spain, in 2016 and 2020, respectively. His research interests include vehicular networking, protection of vulnerable road users, and intelligent transport systems.

Markus Rydeberg obtained an M.Sc. in Data Science and Engineering from the School of Information Technology at Halmstad University in 2023. His master's thesis was on protection of Vulnerable Road Users.

Linnéa Olsson obtained an M.Sc. in Data Science and Engineering from the School of Information Technology at Halmstad University in 2023. Her master's thesis was on protection of Vulnerable Road Users.

Alexey Vinel [SM´12] is a professor at the Karlsruhe Institute of Technology (KIT), Germany. Before he joined KIT in October 2022, he was a professor at the University of Passau, Germany. Since 2015, he has been a professor at Halmstad University, Sweden (now part-time). His areas of interests include vehicular communications and cooperative autonomous driving. He has led several research projects including the Knowledge Foundation synergy project SafeSmart 2019-2024. He received his Ph.D. degree from the Tampere University of Technology, Finland in 2013. He has been a recipient of Alexander von Humboldt Foundation fellowship in 2008.